J. Fluid Mech. (1981), *vol.* 113, *pp.* 153–186
Printed in Great Britain

Oscillatory and steady convection in a magnetic field

By E. KNOBLOCH,
Department of Physics, University of California, Berkeley
N. O. WEISS
Department of Applied Mathematics and Theoretical Physics, University of Cambridge
AND L. N. DA COSTA
SEPLAN/PR-CNPq-Observatorio Nacional, Rua General Bruce 586,
Rio de Janeiro, Brazil

(Received 25 January 1980 and in revised form 9 December 1980)

Two-dimensional convection in a Boussinesq fluid in the presence of an imposed magnetic field is described in terms of a simplified model, which is exact to second order in the amplitude of the motion and appears to be qualitatively correct for larger amplitudes. If the ratio of the magnetic diffusivity to the thermal diffusivity is sufficiently small and the imposed magnetic field is sufficiently large, convection sets in when $r = r^{(o)}$ as overstable oscillations, which grow in amplitude as the normalized Rayleigh number r is increased. There is also a branch of steady solutions that bifurcates from the static equilibrium at $r = r^{(e)} > r^{(o)}$ and stable steady solutions exist for $r > r_{\min}$. For certain choices of parameters subcritical steady convection, with $r_{\min} < r^{(e)}$, is found and the oscillatory branch ends on the unstable portion of the steady branch, where the period of the oscillations becomes infinite. In some circumstances there may be a bifurcation from symmetrical to asymmetrical oscillations, followed by a sequence of bifurcations at each of which the period doubles. Other choices of parameters allow only supercritical convection with r increasing monotonically on the steady branch; if convection first appears as overstable oscillations the steady branch is then unstable for $r^{(e)} < r < r_{\min}$ and there is a Hopf bifurcation at $r = r_{\min}$. This complicated pattern of behaviour is consistent with the results of numerical experiments on the full two-dimensional problem.

1. Introduction

At the surface of a star like the Sun energy is carried outwards by convection. In sunspots, where there are strong local magnetic fields, normal convection is suppressed and only oscillatory motion can occur. It is important, though by no means straightforward, to establish what field strength is needed to inhibit normal convection. This situation can be modelled by considering a horizontal layer containing a Boussinesq fluid whose electrical conductivity is large. Suppose that the layer is permeated by a uniform magnetic field: then the field can support hydromagnetic oscillations, which decay through viscous and ohmic dissipation. These oscillations may, however, be maintained if the layer is heated from below. As the rate of heating is increased, the oscillations grow in amplitude until they eventually give way to steady convection. Such behaviour is typical of systems where stabilizing and destabilizing effects

compete (Spiegel 1972). The aim of this paper is to relate nonlinear solutions to linear theory and to explain the transition from oscillatory to steady motion in the nonlinear regime.

Although it is possible to solve the relevant partial differential equations numerically in certain idealized geometries, this transition cannot be explored with adequate precision. We therefore construct a set of coupled, nonlinear ordinary differential equations with solutions that reproduce the essential features of solutions to the full system. This simplified model is far easier to solve: steady solutions can be written down at once and their stability can be investigated analytically, while time-dependent solutions are readily computed. Thus we are able to isolate the various paths by which periodic and steady solutions merge, and to relate linear to nonlinear results.

The development of two-dimensional convection in a magnetic field has been investigated in a series of numerical experiments (Weiss 1981*a*, *b*) and similar results have been obtained for axisymmetric cells (Galloway & Moore 1979). In the regime of interest the static, conducting solution becomes unstable when the normalized Rayleigh number r (defined in equation (2.16) below) exceeds a critical value $r^{(o)}$. A branch of oscillatory solutions bifurcates from this point (*cf.* figure 1) and terminates shortly after the appearance of steady, finite-amplitude convection at $r = r_{\min}$. Non-oscillatory solutions bifurcate from the conducting state when $r = r^{(e)}$ but $r_{\min}$ may be less than $r^{(e)}$, as in figure 1(*a*). Subcritical steady convection, with $r < r^{(e)}$, is an important feature of this problem and is easily explained. Once convection starts, magnetic flux is concentrated at the edges of the cell (Weiss 1966), thereby facilitating motion in the field-free central region. Flux expulsion therefore allows steady subcritical convection: conversely, any satisfactory model of convection in a magnetic field must allow for the formation of lateral sheets of flux in two dimensions, or isolated tubes in three. With different choices of parameters, $r_{\min}$ may be greater than $r^{(e)}$, as in figure 1(*c*). It is tempting to postulate, in both cases, an unstable continuation of the steady branch from $r_{\min}$ to $r^{(e)}$, to which the oscillatory branch is somehow linked, but such conjectures cannot be confirmed from numerical solutions to the full problem.

To construct a simplified model of two-dimensional magnetoconvection we expand the dependent variables as truncated Fourier series in space and then adopt the minimal representation such that (i) linear results are identical with those for the full problem, (ii) the velocity remains finite for all finite values of r and (iii) some effects of flux expulsion are included. This is achieved with a fifth-order system of ordinary differential equations which possesses both periodic and steady solutions and allows subcritical convection. Moreover, the representation is just that which reproduces results obtained by modified perturbation theory, to second order, for the full problem. This procedure is similar to that followed by Veronis (1965, 1966) in studying the effects of solutes and rotation on convection. The model equations for thermosolutal convection have been studied in some detail (Siegmann & Rubenfeld 1975; Rubenfeld & Siegmann 1977; Da Costa, Knobloch & Weiss 1981) and yield results that are similar to those presented here. The limitations of this procedure are discussed by Da Costa *et al.* (1981).

In § 2 we derive the fifth-order system. Then we summarize the stability properties of the static solution and results for small-amplitude convection. Next, we present some results for the full two-dimensional problem and then obtain nonlinear steady solutions for the model problem and investigate their stability. Time-dependent

solutions, computed numerically, are described in §§6–8. Although the model is a rigorously valid approximation to the full problem only when the velocity is very small, the solutions do reproduce the relevant properties of two-dimensional convection. They also exhibit an extraordinary variety of behaviour: in particular, we show explicitly how oscillatory solutions either bifurcate from the steady solution or else approach it as their period grows infinite. In conclusion, we summarize the results and use them to explain features of the two-dimensional problem. Although our discussion focuses on magnetoconvection, much of it holds also for other double-diffusive systems (Spiegel 1972) and most notably for thermohaline convection. In this paper we confine ourselves to explaining the behaviour of a complicated fluid system; certain more mathematical points are taken up in a parallel study of the thermosolutal problem (Da Costa *et al.* 1981).

2. Derivation of the model

The equations describing thermal convection in a conducting fluid in the presence of a magnetic field (Chandrasekhar 1961; Weiss 1977) are:

$$\frac{\partial \mathbf{u}}{\partial t} + (\mathbf{u}.\nabla)\,\mathbf{u} = -\frac{1}{\rho_0}\nabla p - \frac{\rho}{\rho_0} g\mathbf{e}_z + \frac{1}{\mu_0 \rho_0}(\nabla \wedge \mathbf{B}) \wedge \mathbf{B} + \nu \nabla^2 \mathbf{u}, \tag{2.1}$$

$$\partial T/\partial t = -\nabla.(T\mathbf{u}) + \kappa \nabla^2 T, \tag{2.2}$$

$$\partial \mathbf{B}/\partial t = \nabla \wedge (\mathbf{u} \wedge \mathbf{B}) + \eta \nabla^2 \mathbf{B}, \quad \nabla.\mathbf{B} = 0, \tag{2.3}$$

where in the Boussinesq approximation $\nabla.\mathbf{u} = 0$ and $\rho/\rho_0 = 1 - \alpha(T - T_0)$. Here $\mathbf{u}$ is the velocity, T the temperature and $\mathbf{B}$ the magnetic field; the density ρ is equal to ρ_0 at the reference temperature T_0; and the constants ν, κ, η, μ_0 and α are respectively the viscous, thermal and magnetic diffusivities, the magnetic permeability and the coefficient of thermal expansion. We have taken gravity to act downwards with the constant acceleration g, $\mathbf{e}_z$ being a unit vector in the vertical z direction, and we consider a layer of fluid confined between fixed horizontal planes at $z = 0$, h. A fixed temperature difference ΔT is maintained across the layer and, in the absence of any motion, there is a uniform, externally imposed magnetic field $\mathbf{B}_0 = B_0 \mathbf{e}_z$.

In what follows we shall restrict our attention to two-dimensional convection such that the motion and the magnetic field lie in the (x, z)-plane only, with all the dependent variables independent of the third co-ordinate y. As usual we shall write equations (2.1)–(2.3) in a non-dimensional form by scaling them relative to the thermal conduction time. Thus we scale t by h^2/κ, $\mathbf{u}$ by κ/h, x and z by the separation h, T by ΔT and $\mathbf{B}$ by B_0. Hereafter the symbols t, $\mathbf{u}$, x, z, T and $\mathbf{B}$ will refer to the corresponding dimensionless quantities. For the present configuration it is convenient to eliminate the pressure p from the equation of motion by taking the curl of (2.1) and to express the result in terms of the stream function $\psi(x, z, t)$ and the flux function $A(x, z, t)$ defined by

$$\mathbf{u} \equiv (u, 0, w) = \left(-\frac{\partial \psi}{\partial z}, 0, \frac{\partial \psi}{\partial x}\right), \quad \mathbf{B} \equiv (B_x, 0, B_z) = \left(-\frac{\partial A}{\partial z}, 0, \frac{\partial A}{\partial x}\right). \tag{2.4}$$

Since the magnetic field is concentrated by the motion into vertical sheets, it is convenient to separate A into a *vertically* averaged flux function $\bar{A}(x, t)$ and a fluctuating

component $A'(x,z,t) \equiv A - \bar{A}$. The temperature $T(x,z,t)$ is similarly separated into a *horizontally* averaged temperature $\bar{T}(z,t)$ and a fluctuating temperature component $T'(x,z,t) \equiv T - \bar{T}$. We then obtain the dimensionless equations

$$\frac{1}{\sigma}\left[\frac{\partial}{\partial t}\nabla^2\psi + \frac{\partial(\psi, \nabla^2\psi)}{\partial(x,z)}\right] = \nabla^4\psi + R\frac{\partial T'}{\partial x} + \zeta Q\frac{\partial(A, \nabla^2 A)}{\partial(x,z)}, \tag{2.5a}$$

$$\frac{\partial T'}{\partial t} + \frac{\partial(\psi, T')}{\partial(x,z)} - \left\langle \frac{\partial(\psi, T')}{\partial(x,z)} \right\rangle_x = \nabla^2 T' - w\frac{\partial \bar{T}}{\partial z}, \tag{2.5b}$$

$$\frac{\partial \bar{T}}{\partial t} + \frac{\partial}{\partial z}\langle wT' \rangle_x = \frac{\partial^2 \bar{T}}{\partial z^2}, \tag{2.5c}$$

$$\frac{\partial A'}{\partial t} + \frac{\partial(\psi, A')}{\partial(x,z)} - \left\langle \frac{\partial(\psi, A')}{\partial(x,z)} \right\rangle_z = \zeta\nabla^2 A' - u\frac{\partial \bar{A}}{\partial x}, \tag{2.5d}$$

$$\frac{\partial \bar{A}}{\partial t} + \frac{\partial}{\partial x}\langle uA' \rangle_z = \zeta\frac{\partial^2 \bar{A}}{\partial x^2}, \tag{2.5e}$$

where the angled brackets in (2.5*b*, *c*) and (2.5*d*, *e*) denote horizontal and vertical averages respectively, and the dimensionless parameters σ, ζ, R and Q are defined by

$$\sigma = \frac{\nu}{\kappa}, \quad \zeta = \frac{\eta}{\kappa}, \quad R = \frac{g\alpha\Delta T h^3}{\kappa\nu}, \quad Q = \frac{B_0^2 h^2}{\mu_0 \rho_0 \eta \nu}. \tag{2.6}$$

These quantities are respectively the two Prandtl numbers, the Rayleigh number and the Chandrasekhar number.

We shall be interested in understanding the nonlinear properties of magneto-convection in a cell of width λ. For convenience we adopt the illustrative stress-free boundary conditions that yield sines and cosines as the eigenfunctions of the linear problem (Chandrasekhar 1961). Thus for the velocity field

$$\begin{aligned} u = \partial^2 u/\partial x^2 = 0 \quad &\text{on} \quad x = 0, \quad x = \lambda, \\ w = \partial^2 w/\partial z^2 = 0 \quad &\text{on} \quad z = 0, \quad z = 1, \end{aligned} \tag{2.7}$$

for the temperature field

$$\begin{aligned} &\bar{T} = 1 \quad \text{on} \quad z = 0, \qquad \bar{T} = 0 \quad \text{on} \quad z = 1, \\ &T' = 0 \quad \text{on} \quad z = 0, \quad z = 1, \qquad \partial T'/\partial x = 0 \quad \text{on} \quad x = 0, \quad x = \lambda, \end{aligned} \tag{2.8}$$

and for the magnetic field

$$\begin{aligned} &\bar{A} = 0 \quad \text{on} \quad x = 0, \qquad \bar{A} = \lambda \quad \text{on} \quad x = \lambda, \\ &A' = 0 \quad \text{on} \quad x = 0, \quad x = \lambda, \qquad \partial A'/\partial z = 0 \quad \text{on} \quad z = 0, \quad z = 1. \end{aligned} \tag{2.9}$$

These boundary conditions allow the concentration of the field into flux sheets at the sides of the cell without requiring magnetic boundary layers at the top and bottom. Equations (2.5)–(2.9) define the problem solved numerically by Weiss (1981*a*, *b*).

To construct a simplified model of this basic problem we follow the procedure introduced by Veronis (1965). The stream functions, the flux function and the temperature are expanded as Fourier series in x and z, and only the leading terms are

retained. The velocity field consistent with the boundary conditions (2.7) is then described by

$$\psi = 2(2p)^{\frac{1}{2}} \frac{\lambda}{\pi} \sin\frac{\pi x}{\lambda} \sin \pi z \, a(\tau), \tag{2.10}$$

where τ is the time measured in terms of the thermal decay time for the fundamental mode,

$$\tau = pt, \quad p = \pi^2(1 + 1/\lambda^2), \tag{2.11}$$

and the constants have been inserted for later convenience. In the presence of motion the horizontally averaged temperature $\bar{T}$ acquires a bimodal deviation from the conductive temperature distribution $\bar{T} = 1 - z$ that corresponds to the formation of thermal boundary layers at top and bottom. Thus we set

$$\bar{T} = 1 - z - \pi^{-1} \sin 2\pi z \, c(\tau). \tag{2.12}$$

In order to represent the concentration of the initially uniform magnetic field into flux sheets at both sides of the cell we let

$$\bar{A} = x + \frac{\lambda}{\pi} \sin\frac{2\pi x}{\lambda} e(\tau). \tag{2.13}$$

Finally, the thermal and magnetic fluctuations are each described by a single mode, corresponding to the eigenfunctions of the linearized problem, so that

$$T' = 2(2/p)^{\frac{1}{2}} \cos\frac{\pi x}{\lambda} \sin \pi z \, b(\tau) \tag{2.14}$$

and

$$A' = 2(2/p)^{\frac{1}{2}} \lambda \sin\frac{\pi x}{\lambda} \cos \pi z \, d(\tau). \tag{2.15}$$

Equations (2.10)–(2.15) describe the main physical features of the system that we wish to model.

The differential equations are derived by substituting these expressions into (2.5) and consistently neglecting all terms generated that involve higher harmonics. For example, in (2.5*a*) we neglect the term proportional to $\sin(3\pi x/\lambda) \sin \pi z$ that is generated from the product $\sin(\pi x/\lambda) \cos(2\pi x/\lambda) \sin \pi z$. With the definitions

$$r = \frac{\pi^2}{\lambda^2 p^3} R, \quad q = \frac{\pi^2}{p^2} Q, \quad \varpi = \frac{4\pi^2}{p}, \tag{2.16}$$

so that $0 \leqslant \varpi \leqslant 4$, we obtain

$$\dot{a} = \sigma[-a + rb + \zeta q d\{(\varpi - 3)e - 1\}], \tag{2.17a}$$

where the dot denotes differentiation with respect to τ. Similarly, from (2.5*b–e*), we obtain the equations

$$\dot{b} = -b + a(1 - c), \tag{2.17b}$$

$$\dot{c} = \varpi(-c + ab), \tag{2.17c}$$

$$\dot{d} = -\zeta d + a(1 - e), \tag{2.17d}$$

$$\dot{e} = -(4 - \varpi)\zeta e + \varpi a d. \tag{2.17e}$$

The truncation leading to the above equations is consistent in that no other low-order harmonics are generated by the substitutions (2.10)–(2.15). It may also be observed that this truncation automatically conserves the uniform field component even if the boundary condition (2.9) is not explicitly applied.

Equations (2.17) are the basic set that will be studied in this paper. These equations possess two significant properties. First, the divergence of the flow in phase space,

$$\frac{\partial \dot{a}}{\partial a}+\frac{\partial \dot{b}}{\partial b}+\frac{\partial \dot{c}}{\partial c}+\frac{\partial \dot{d}}{\partial d}+\frac{\partial \dot{e}}{\partial e}=-[\sigma+(1+\varpi)+\zeta(5-\varpi)], \tag{2.18}$$

is always negative and so the solutions are attracted to a set of measure zero in the phase space: this may be a fixed point, a limit cycle or a strange attractor. Second, the equations have an important symmetry, for they are unchanged if the signs of a, b and d are reversed while c and e are left unchanged. They resemble the equations derived by Veronis (1965, 1966) for other double-diffusive systems but there is one crucial difference, for the nonlinear Lorentz force now appears in the equation of motion (2.17a). When $q = 0$, equations (2.17a–c) can be transformed to the system that was studied by Lorenz (1963). Above we have attempted to justify their derivation on physical grounds, without restriction on the amplitude of the convective motions. More generally, the Fourier expansion in x and z leads to an infinite set of coupled nonlinear ordinary differential equations. The truncation (2.10)–(2.15) does in fact include just those Fourier components that appear when a is small but the truncated system (2.17) can be rigorously justified as an approximation to (2.5) only for

$$\max(a, a/\sigma, a/\zeta) \ll 1. \tag{2.19}$$

The physical arguments presented above do, however, suggest that the qualitative validity of (2.17) extends to far larger amplitude. This will indeed be demonstrated below by direct comparison of solutions to the two systems. Consequently the model equations merit detailed investigation in an attempt to understand the qualitative properties of the various possible solutions to the full nonlinear equations.

3. Bifurcations from the static solution

The variables a, b and d, defined in (2.10), (2.14) and (2.15), are just the coefficients of the modes that appear as eigenfunctions of the linear stability problem that can be derived from (2.5), (2.7), (2.8) and (2.9) (*cf.* Chandrasekhar 1961). Since the equations (2.17) contain all linear relations between these modes, the linear problem derived from the model equations must be identical to that for the full system, as required in § 1. Moreover, it can easily be shown that the only additional Fourier modes generated by nonlinear interactions between the modes that appear in the linear system are just those that are included in (2.12) and (2.13). Thus the results obtained by modified perturbation theory will, to second order, be identical for the full two-dimensional system and for the model equations (2.17). These results will be summarized in this section.

(*a*) *Linear stability theory*

Equations (2.17) admit the trivial solution $a = b = c = d = e = 0$ that corresponds to pure conduction of heat, with no fluid motion present. The linear stability properties of this static solution are obtained from (2.17) upon neglecting all quadratic terms

and seeking solutions of the form $\exp s\tau$. No instability arises from the decoupled equations for c and e, while the remaining three equations yield the cubic dispersion relation (Chandrasekhar 1961; Weiss 1964)

$$s^3+(1+\sigma+\zeta)\,s^2+[\sigma(1-r+\zeta q)+\zeta(1+\sigma)]\,s+\sigma\zeta(1-r+q)=0. \tag{3.1}$$

In particular, one of the eigenvalues s vanishes (corresponding to an exchange of stabilities) at

$$r^{(e)}=1+q. \tag{3.2}$$

Thus the normalized Rayleigh number $r=1$ at the onset of convection in the field-free case. The Rayleigh number at which there is a pair of purely imaginary eigenvalues $s=\pm i\omega_0$ (corresponding to the onset of overstability) is

$$r^{(o)}=(\sigma+\zeta)\left[\frac{1+\zeta}{\sigma}+\frac{\zeta}{1+\sigma}q\right], \tag{3.3}$$

while the corresponding frequency of oscillations is given by

$$\omega_0^2=-\zeta^2+\left(\frac{1-\zeta}{1+\sigma}\right)\sigma\zeta q. \tag{3.4}$$

Since

$$r^{(e)}-r^{(o)}=\omega_0^2\Delta/\sigma\zeta, \tag{3.5}$$

where $\Delta=1+\sigma+\zeta$, ω_0 is real if and only if overstability sets in prior to the exchange of stabilities. This requires that q be greater than

$$q_0=\frac{\zeta}{\sigma}\left(\frac{1+\sigma}{1-\zeta}\right), \quad \zeta<1; \tag{3.6}$$

if $q<q_0$ or if $\zeta>1$, overstability cannot occur. We may therefore distinguish the following two cases.

(i) $\omega_0^2<0$. In this case as r is increased there is a simple bifurcation at $r^{(e)}$ and convection first sets in as a direct (or monotonically growing) mode.

(ii) $\omega_0^2>0$ ($r^{(o)}<r^{(e)}$). Here there is a Hopf bifurcation at $r^{(o)}$ and convection first sets in as an overstable mode. If $r^{(i)}$ is the lowest value of r at which s is purely real (Danielson 1961; Weiss 1964), then for $r<r^{(o)}$ (3.1) has two complex-conjugate eigenvalues with negative real parts while for $r^{(o)}<r<r^{(i)}$ the eigenvalues have positive real parts; for $r^{(i)}<r<r^{(e)}$ there are two positive real eigenvalues, one of which becomes negative for $r>r^{(e)}$. The third eigenvalue of (3.1) is always negative and therefore uninteresting. This second case is the one of principal concern in this paper.

(*b*) *Modified perturbation theory*

Let us first consider the simple bifurcation at $r^{(e)}$. In the neighbourhood of $r^{(e)}$ there is a triplet of steady solutions, one of which is the static solution (which is always unstable for $r>r^{(e)}$). The other two are finite-amplitude solutions which, owing to the symmetry of (2.17), differ only in the sign of a, b and d. We may investigate the behaviour of the two branches of non-trivial steady solutions in the neighbourhood of $r^{(e)}$ in terms of the velocity a by setting

$$r=r^{(e)}+r_2^{(e)}a^2+O(a^4) \tag{3.7}$$

for $a^2 \ll 1$. We then find that

$$r_2^{(e)} = 1 + q + \frac{(2-\varpi)\varpi q}{(4-\varpi)\zeta^2}. \tag{3.8}$$

This result is equivalent to that for the full problem, originally obtained by Veronis (1959, in a footnote) and quoted by Weiss (1981*a*).

From (3.8) we see that the branch of steady solutions bifurcates towards larger r ($r_2^{(e)} > 0$) for all $\varpi \leqslant 2$. In particular, for the case of interest when overstability sets in first and $\zeta \ll 1$, $r_2^{(e)}$ is much larger when $\varpi < 2$ (i.e. vertically elongated cells with $\lambda < 1$) than when $\varpi = 2$ (square cells). In the latter marginal case the branch bifurcates from $r^{(e)}$ almost vertically when a^2 is plotted against r. For $\varpi > 2$ (horizontally flattened cells) the branch bifurcates towards smaller r ($r_2^{(e)} < 0$) when $\zeta \ll 1$. Hence the imposed geometry of the convection cells is very important in determining the behaviour of the direct modes in the neighbourhood of the simple bifurcation.

The above results are unaffected by the presence of overstability. When $\omega_0^2 < 0$, the stability of the steady branch in the neighbourhood of $r^{(e)}$ is determined solely by the sign of $r_2^{(e)}$. These stability properties, which are crucial for a proper understanding of the global stability of the steady branch, are, however, changed when overstability occurs first. We postpone discussing them until §4.

Finite-amplitude oscillatory modes can be treated similarly. When $\omega_0^2 > 0$, we may use modified perturbation theory to examine the behaviour of the branch of oscillatory solutions in the neighbourhood of the Hopf bifurcation at $r^{(o)}$. Following Veronis (1959), we assume that motion is periodic, with period $2\pi/\omega$, and expand both the frequency ω and the Rayleigh number r in powers of a small parameter ϵ related to the amplitude of the oscillations:

$$\begin{aligned} \omega &= \omega_0 + \epsilon\omega_1 + \epsilon^2\omega_2 + \ldots, \\ r &= r^{(o)} + \epsilon r_1^{(o)} + \epsilon^2 r_2^{(o)} + \ldots, \\ a &= \epsilon a_1 + \epsilon^2 a_2 + \epsilon^3 a_3 + \ldots, \end{aligned} \tag{3.9}$$

and similarly for b, c, d and e. A procedure for determining whether the bifurcation is subcritical is outlined in the appendix. We find that $\omega_1 = r_1^{(o)} = 0$ and that $r_2^{(o)}$ may be either positive or negative. It can be shown that $r_2^{(o)} > 0$ for square cells ($\varpi = 2$) but that, for sufficiently slender or sufficiently flat cells, subcritical bifurcation is possible. The stability of the oscillatory branch in the neighbourhood of $r^{(o)}$ is described by the Hopf bifurcation theorem (Hopf 1942; Sattinger 1973; Marsden & McCracken 1976). According to this theorem the oscillatory solutions are stable if the Hopf bifurcation is supercritical ($r_2^{(o)} > 0$) and unstable if it is subcritical ($r_2^{(o)} < 0$).

We have already noted that these finite-amplitude results are identical for the full system and for the model equations. Although the two systems diverge at third order, the solvability condition involves only those modes that are already present: hence $r_2^{(e)}$, $r_2^{(o)}$ and ω_2 are the same for both systems. This agreement is a straightforward consequence of the fact that the modes included, on physical grounds, in (2.12) and (2.13) are the only additional modes that appear in second order from the perturbation expansion. Furthermore, it is easier to obtain finite-amplitude results (especially for time-dependent convection) from (2.17) than from the full equations.

This comparison suggests a systematic procedure for generating higher-order systems of ordinary differential equations. The modes that have to be included are

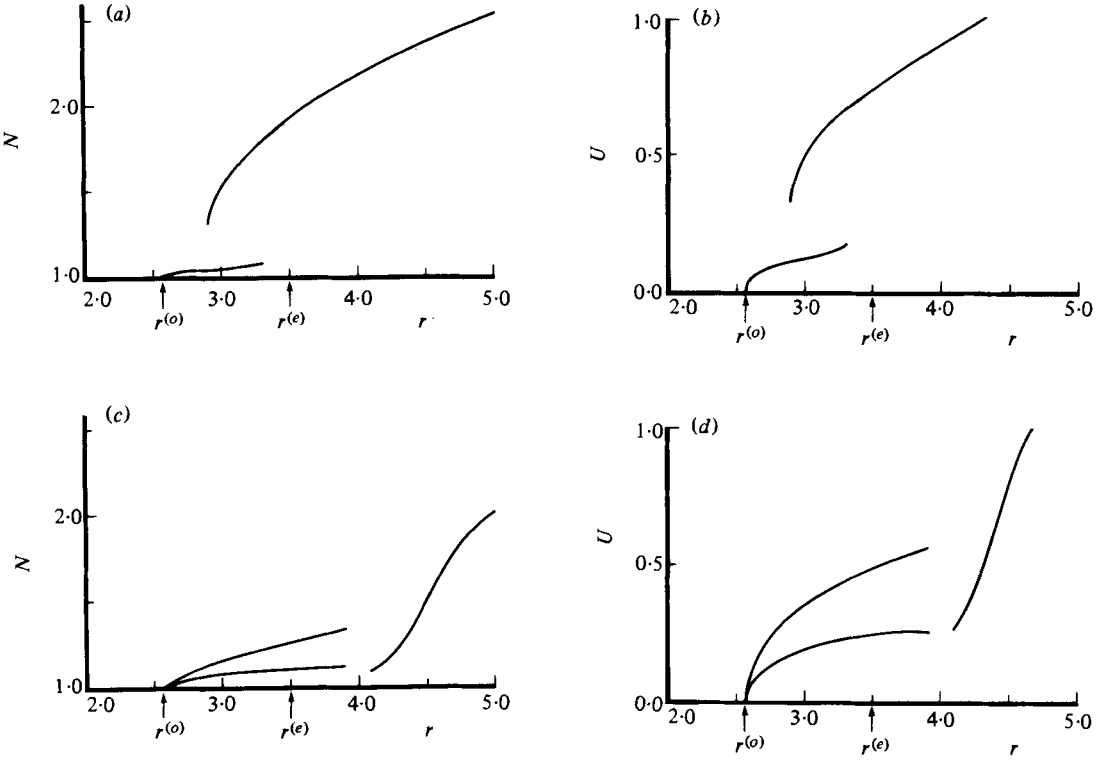

FIG. 1. Results for the full two-dimensional problem with $q = 2{\cdot}5$, $\sigma = \zeta = \frac{1}{5}$. Subcritical steady convection with $\lambda = 1$: (*a*) the Nusselt number N and (*b*) the scaled root-mean-square velocity U, as functions of r; for oscillatory solutions only the maximum values are plotted. Supercritical convection with $\lambda = \frac{1}{2}$: (*c*) $N(r)$ and (*d*) $U(r)$; for oscillatory solutions both maximum and average values are plotted.

precisely those that appear as modified perturbation theory is applied to higher order. It is possible to construct an eleventh-order extension of (2.17) in this way. We should, however, bear in mind that the radius of convergence of the perturbation expansion is limited by (2.19) and that the addition of a few more modes will be effective only if some new physical process is represented. Otherwise there is no satisfactory choice that lies between the minimal system (2.17) and including enough modes to provide an accurate solution of the full equations (2.5).

4. Properties of steady convection

The nonlinear partial differential equations (2.5) that govern two-dimensional convection can be integrated numerically on a computer and Weiss (1981*a*) has obtained families of solutions as r is increased for different choices of the parameters ζ and q. These results are inevitably incomplete and it is impossible to investigate the entire five-dimensional parameter space. The numerical experiments do, however, yield both steady and oscillatory solutions; they also reveal behaviour that is bewilderingly complex.

To illustrate these problems we show the results of two series of numerical experiments. The vigour of convection can be measured in terms of either the heat flux or the

kinetic energy. It is convenient to introduce a normalized heat flux, given by the Nusselt number $N = -\partial\bar{T}/\partial z$, evaluated at $z = 0$; in the absence of motion $N = 1$ and, from (2.12), $N = 1 + 2c$ for small-amplitude convection. To facilitate comparison with subsequent results, we define a normalized root-mean-square velocity U such that

$$U^2 = (\lambda^2/2\pi^2)(1+\lambda^2)^{-2}\langle \mathbf{u}^2 \rangle, \tag{4.1}$$

where the angled brackets denote a spatial average; for small-amplitude convection $U = a$. In figure 1, both N and U are plotted against r; for some oscillatory solutions the maximum values and the time-averaged values are shown. The two series of experiments both have $q = 2{\cdot}5$, $\sigma = \zeta = 0{\cdot}2$; hence convection sets in as overstable oscillations and $r^{(o)} \simeq 2{\cdot}57$, $r^{(e)} = 3{\cdot}5$ in each case. For the runs in figures 1 (*a*, *b*), $\lambda = 1$ ($\varpi = 2$) while, for those in figures 1 (*c*, *d*), $\lambda = \frac{1}{2}$ ($\varpi = 0{\cdot}8$). It follows from (3.8) that $r_2^{(e)} > 0$ in each case.

Figures 1 (*a*, *b*) show that convection first appears at $r^{(o)}$ but the oscillatory solutions are ineffectual at transporting heat: the Nusselt number $N < 1{\cdot}1$, while $U < 0{\cdot}23$. Convective transport of heat becomes significant with the appearance of steady solutions, which exist for all $r > r_{\min} \simeq 2{\cdot}9$. For square cells, therefore, steady convection first appears, with a finite amplitude, at $r_{\min} < r^{(e)}$. For $r^{(o)} < r < r_{\min}$ only oscillatory solutions exist. As r is increased, the period of the oscillations rises and for $r > 3{\cdot}3$ there are no persistent oscillatory solutions. (In the run with $r = 3{\cdot}3$, the solution paused briefly with $N \simeq 1{\cdot}08$ before making an abrupt transition to steady convection with $N \simeq 1{\cdot}78$.)

Figures 1 (*c*, *d*) look quite different. Steady solutions are found for $r > r_{\min} \simeq 4{\cdot}0$. For $r = 4{\cdot}1$ the numerical results showed transient oscillations about a steady state; this solution was used to provide initial values for a run with $r = 3{\cdot}9$, which developed large-scale oscillations with a reversal of the flow after each half-cycle. When $\lambda = \frac{1}{2}$, therefore, oscillatory solutions persist beyond $r^{(e)}$, while stable steady solutions only appear at a value of r that is distinctly greater than $r^{(e)}$. The branch of oscillatory solutions, which bifurcates from $r^{(o)}$, continues up to $r \simeq r_{\min}$, though the convective heat transport remains small. At $r = 4{\cdot}1$ only steady solutions were obtained and N rose rapidly as r was increased.

It is natural to assume that the steady branch in figure 1 (*c*) bifurcates from $r^{(e)}$ and that the stable part, with $r > r_{\min}$, is preceded by unstable steady solutions in the range $r^{(e)} < r < r_{\min}$. Similarly, we may suppose that the steady branch in figure 1 (*a*) is also linked to $r^{(e)}$ by an unstable part. Since $r_2^{(e)} > 0$, the unstable part must have a positive slope at the bifurcation and so there must be two turning points on the steady branch. Such conjectures cannot be confirmed without calculating the relevant solutions and investigating their stability. Again, the oscillatory branches terminate when r is slightly greater than $r_{\min}$, with $\bar{N}$ close to the value on the steady branch, and the period of the oscillations increases rapidly towards the end. Yet it is not obvious how the transition from oscillatory to steady motion takes place.

In order to resolve these problems we have to fall back on a simpler and more tractable system of equations. Fortunately, the behaviour of solutions to the model equations (2.17) closely follows that depicted in figure 1. The ordinary differential equations have the great advantage that steady solutions can be written down immediately and their stability can easily be studied. Nonlinear time-dependent solutions are readily computed and the transition from an oscillatory to a steady

branch can be followed and explained. The close similarity between solutions to the model equations and numerical results for the full problem provides a sufficient justification for studying the former in some detail. In this section we present the steady solutions and classify different types of behaviour. Then we discuss the stability of the steady solutions, reserving mathematical details for the following section.

Equations (2.17) admit a non-trivial steady solution defined for all amplitudes a of the motion. This solution is given by

$$b = \frac{a}{1+a^2}, \quad c = \frac{a^2}{1+a^2}, \quad d = \frac{\mu\zeta^{-1}a}{\mu+a^2}, \quad e = \frac{a^2}{\mu+a^2}, \tag{4.2}$$

where a satisfies the equation

$$r-1 = a^2 + \frac{\mu(1+a^2)[\mu+(4-\varpi)a^2]}{(\mu+a^2)^2}q, \tag{4.3}$$

and the parameter μ is given by

$$\mu = (4-\varpi)\zeta^2/\varpi. \tag{4.4}$$

Thus steady motion is possible only for $r \geqslant 1$ and for large Rayleigh numbers (4.3) tends asymptotically to $r = 1+\mu(4-\varpi)q+a^2$, so that we have, approximately,

$$a = \pm r^{\frac{1}{2}}, \quad b = d = 0, \quad c = e = 1. \tag{4.5}$$

Since c, e never exceed unity it follows from (2.11) and (2.12) that $\bar{T}$ and $\bar{A}$ satisfy the realizability conditions $0 \leqslant \bar{T}(z) \leqslant 1$, $0 \leqslant \bar{A}(x) \leqslant \lambda$. However, the vertically averaged magnetic field $d\bar{A}/dx$ reverses at the centre of the cell when $e > \frac{1}{2}$ ($a^2 > \mu$); such a reversal, like the corresponding temperature inversion, is characteristic of two-dimensional convection.

The steady solutions are independent of the Prandtl number σ. Suppose that $\zeta < 1$, $q > \zeta/(1-\zeta)$: then, from (3.6), overstability is precluded if σ is sufficiently small but if σ is increased overstability eventually occurs. The steady solutions are unaffected by this process but their stability properties are profoundly altered. Consequently there is a multitude of cases that have to be considered. In order to simplify the enumeration of different types of behaviour the discussion in this section is largely descriptive and a more formal treatment is deferred to § 5.

First of all, we may classify the different types of steady-solution branches. From (4.3) the solution $r = r(a^2)$ is a single-valued function. Thus $a = 0$ only when $r = r^{(e)}$ and the two steady-solution branches bifurcate from the static solution at $r^{(e)}$, as postulated above. The bifurcation may be towards larger or smaller values of r, depending on the sign of $r_2^{(e)}$. The behaviour of the steady branches for larger amplitudes can be understood by noting that (4.3) may also be written as a cubic equation for $a^2 = a^2(r)$. Hence three possible types of steady solution branches can arise, characterized by having one, two or no turning points. These three types are sketched in figures 2 (a, b and c) respectively: note that a^2 is shown, so that the two solution branches corresponding to $\pm a$ coincide. In type (a) the bifurcation at $r^{(e)}$ is towards smaller r, until a turning point is reached, beyond which r increases with increasing a^2; in (b) the bifurcation at $r^{(e)}$ is towards larger r, until a first turning point is reached at $r > r^{(e)}$, beyond which r decreases with increasing a^2 to a second turning point, before finally increasing again (*cf.* Proctor & Galloway 1979); in (c) the bifurcation is towards larger r and r increases monotonically with a^2. Steady solutions of type (a)

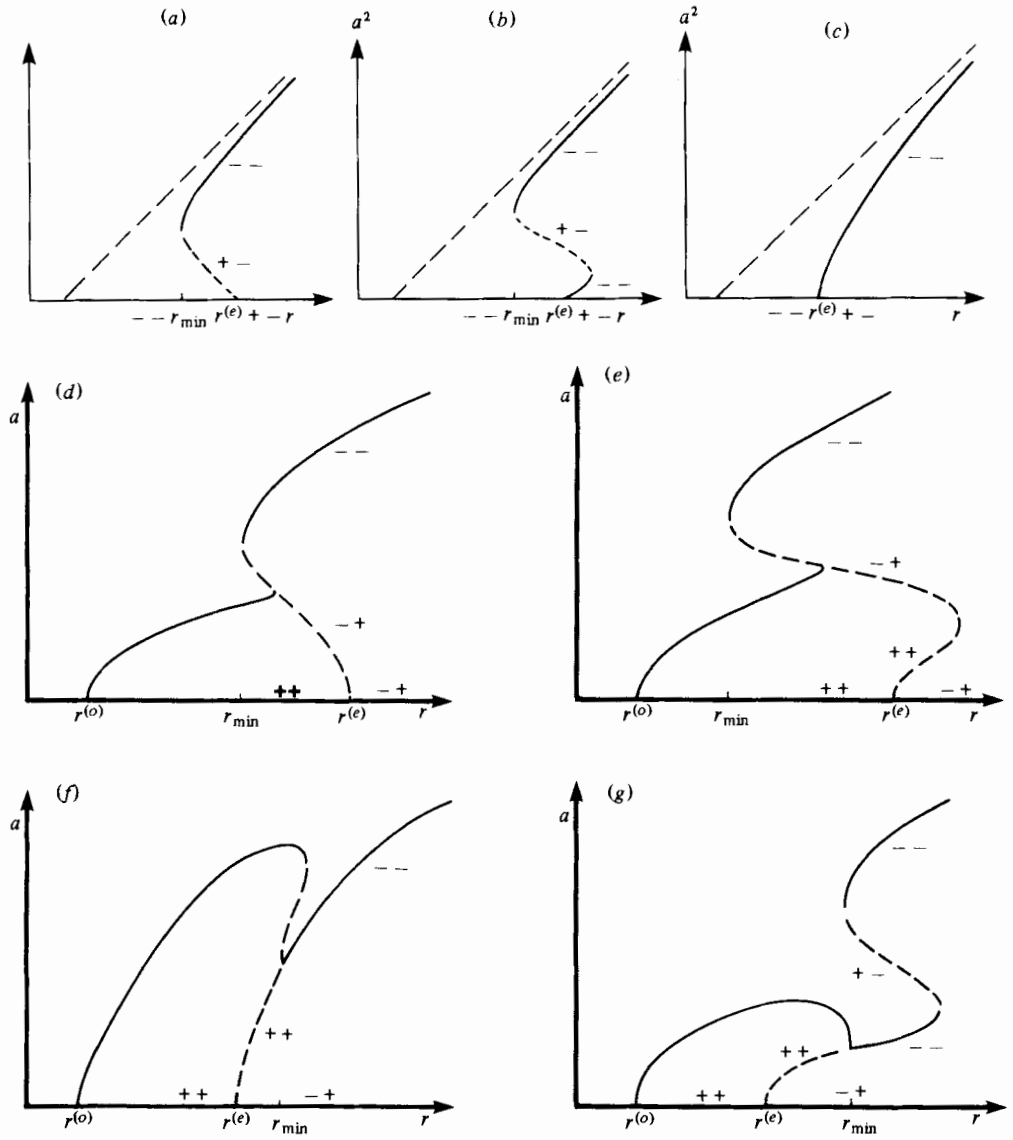

FIGURE 2. Sketches showing the six standard types of solution for the model problem. The first three show a^2 as a function of r when there are no oscillatory solutions and the branch of steady solutions has (*a*) one, (*b*) two and (*c*) no turning points. The next four sketches show $|a|$ (for steady solutions) and the r.m.s. value of a (for oscillatory solutions) as functions of r when $\omega_0^2 > 0$. The steady branches in (*d*), (*e*), (*f*) and (*g*) are similar to those in (*a*), (*b*), (*c*) and (*b*) respectively but their stability properties are altered by the presence of an oscillatory branch. Linear stability is indicated by the signs of the real parts of the two important eigenvalues. The first sign is that of the small eigenvalue arising from the bifurcation at $r^{(e)}$; the second sign corresponds to the important non-zero eigenvalue at $r^{(e)}$, which is negative when $\omega_0^2 < 0$ and positive when $\omega_0^2 > 0$ ($r^{(e)} > r^{(o)}$). The other three eigenvalues have negative real parts and are not indicated. The broken portions of the curves indicate unstable solutions.

with $r < r^{(e)}$ will be called subcritical solutions, while those of type (*c*) will be called supercritical, since $r > r^{(e)}$ for all $a^2 > 0$.

As already mentioned, the stability properties of the steady solutions depend critically on whether or not the simple bifurcation at $r^{(e)}$ is preceded by a Hopf bifurcation at $r^{(o)}$. We consider first the simpler case in which convection sets in as a direct mode ($\omega_0^2 < 0$). The linear stability of the steady-solution branch is described by a quintic dispersion relation for the eigenvalues s. One of the five eigenvalues is always negative. At large r there may be a bifurcation of the type described by Lorenz (1963). If we ignore this possibility, for reasons discussed by Da Costa *et al.* (1981), then two other eigenvalues have negative real parts. We therefore restrict our attention to the remaining pair, which are real at least in the neighbourhood of $r^{(e)}$ and can change sign. When $r_2^{(e)} < 0$ the bifurcation at $r^{(e)}$ is subcritical and the two steady-solution branches are unstable in the neighbourhood of $r^{(e)}$ (Poincaré 1885; Jeans 1928). Conversely, when $r_2^{(e)} > 0$ the supercritical bifurcation is stable. Thus in the former case there is a small positive eigenvalue associated with the linear instability of the steady branch, while in the latter case there is a small negative eigenvalue. The sign of this eigenvalue is determined by the nature of the bifurcation, and its magnitude is small because it must vanish at the bifurcation. The sign of the remaining eigenvalue is the same as that of the corresponding eigenvalue associated with the stability of the *static* solution, and its magnitude is typically large. When $\omega_0^2 < 0$, this latter eigenvalue is negative.

The following discussion relies heavily on the result that in linear stability theory the only neutrally stable points are $r = r^{(e)}$ and the turning points. At these points an eigenvalue s passes singly through zero, so that s must be real in their neighbourhood. This result can be proved quite generally (*cf.* Da Costa *et al.* 1981), and is demonstrated explicitly in § 5. With it we are in a position to describe the stability properties of the steady solutions in the case $\omega_0^2 < 0$. Since the monotonic branch present in type (*c*) is stable in the neighbourhood of $r^{(e)}$ and since there are no turning points or Hopf bifurcations (if the possible Lorenz bifurcation at large r is excluded) it must be stable for all r. Subcritical steady convection of type (*b*) can be produced by reducing the value of the parameter ζ. Since the dependence of the eigenvalues s on ζ is continuous, it follows that the upper steady branch remains stable until one of the eigenvalues can pass through zero at the left turning point. Moreover, since (*b*) is produced *via* an inflection point, it must be the same eigenvalue that changes sign at the right turning point. Hence in (*b*) the small negative eigenvalue near $r^{(e)}$ passes through zero at the right turning point and remains positive on the portion of the steady-solution branch between the two turning points before passing through zero at the left turning point. Since the real parts of the other four eigenvalues remain negative the only unstable part of the branch is that between the two turning points. Now the type (*a*) solution may be obtained from type (*b*) by increasing ϖ. By continuity in ϖ the upper steady branch remains stable, so that the small positive eigenvalue present near $r^{(e)}$ first increases along the subcritical steady branch before decreasing again, and passing through zero at the turning point. Note that once the stability of the upper steady branch is established it becomes clear that a positive eigenvalue must become negative at the left turning point, rather than a second eigenvalue becoming positive. These stability properties are summarized in figures 2(*a*)–(*c*), where $\pm$ signs indicate the signs of the two relevant eigenvalues.

Finally, we discuss the linear stability of the steady-solution branch in the case when overstability precedes the exchange of stabilities ($\omega_0^2 > 0$). Some care must be taken in applying the general stability results because now as r is increased through $r^{(e)}$ one eigenvalue of the linear problem becomes *negative*, while another remains large and positive (§3). The behaviour of the eigenvalue that is responsible for the bifurcation at $r^{(e)}$ is therefore opposite to that described above; consequently the small eigenvalue on the steady branches becomes negative when $r_2^{(e)} < 0$, and positive when $r_2^{(e)} > 0$. (This result is established explicitly in §5.) The steady-solution branches with $r_2^{(e)} < 0$ are still unstable, but now with a single large positive eigenvalue, while the branches with $r_2^{(e)} > 0$ are doubly unstable, with one small and one large positive eigenvalue.

Figures 2(*d–g*) show four different types of behaviour for the case when convection sets in *via* a Hopf bifurcation at $r^{(o)}$. For each type the root-mean-square value of a (for oscillatory solutions) and $|a|$ (for steady solutions) are sketched as functions of r. We shall now discuss the stability of these four types of steady branch. Consider first type (*d*): here the bifurcation at $r^{(e)}$ is unstable with one large positive eigenvalue that passes through zero at the turning point, the real parts of the other eigenvalues remaining negative in order that the upper steady branch be stable (see below). There is no Hopf bifurcation of the steady branch, and so nothing else can happen. However, in type (*f*) there always has to be a Hopf bifurcation if the steady branch is to be stable at large r. This is because the bifurcation at $r^{(e)}$ is doubly unstable, with one small and one large positive eigenvalue: in the absence of turning points the only way that two real unstable eigenvalues can become stable as r is increased is by first becoming equal and splitting into a conjugate pair of eigenvalues with positive real parts, which subsequently decrease to zero at a Hopf bifurcation. If σ is now decreased so that $r^{(o)}$ gets closer to $r^{(e)}$, the bifurcation point moves closer to $r^{(e)}$ until, at $\sigma = \xi/[(1-\zeta)q-\zeta]$, when $r^{(o)} = r^{(e)}$, the bifurcation point disappears and the steady branch is stable. Since in this process the other eigenvalues cannot pass through zero, or become purely imaginary, it follows that the steady branch is indeed stable beyond the Hopf bifurcation. Furthermore, by continuity in the parameters ζ and ϖ it follows that the upper steady branch in type (*d*) is also stable as was assumed above.

If there are two turning points on the steady branch the bifurcation at $r^{(e)}$ is again doubly unstable, with one large and one small eigenvalue, but now there are two possibilities. In type (*e*) the small eigenvalue passes through zero at the first turning point and remains negative thereafter, while the second eigenvalue remains positive until the second turning point, where it too passes through zero. In type (*g*), on the other hand, there is a Hopf bifurcation at $r = r_H$ ($> r^{(e)}$) before the first turning point is reached. Between r_H and the first turning point the steady branch is therefore stable (*cf.* type (*b*)) though it is still unstable between the two turning points. At the first turning point an eigenvalue passes through zero and remains positive until it passes through zero once more at the second turning point. In either case, therefore, the part of the steady branch between the turning points is unstable, while the upper steady branch continues to be stable. The stability properties for types (*d*)–(*g*) are all summarized in figure 2.

We note that the model (2.17) not only provides solutions that are qualitatively similar to those of the full equations (figures 1*a*, *b*), but also enables us to analyse the stability properties of the steady solutions and thereby to gain an understanding of

Type	Conditions	ω_0^2	$r_{\min}$
(*a*)	$r_2^{(e)} < 0$	< 0	r_1
(*b*)	$r_2^{(e)} > 0$, $q > q_1 > 0$, $a_1^2 > 0$	< 0	
	(i) $q > q_2$		r_1
	(ii) $q < q_2$		$r^{(e)}$
(*c*)	$r_2^{(e)} > 0$		
	$q_1 < 0$ or $a_1^2 < 0$ or $0 < q < q_1$, $a_1^2 > 0$	< 0	$r^{(e)}$
(*d*)	$r_2^{(e)} < 0$	> 0	r_1
(*e*)	$r_2^{(e)} > 0$, $q > q_1 > 0$, $a_1^2 > 0$		
	No Hopf bifurcation	> 0	r_1
(*f*)	$r_2^{(e)} > 0$		
	$q_1 < 0$ or $a_1^2 < 0$ or $0 < q < q_1$, $a_1^2 > 0$	> 0	r_H ($> r^{(e)}$)
(*g*)	$r_2^{(e)} > 0$, $q > q_1 > 0$, $a_1^2 > 0$	> 0	
	(i) $r_H > r_1$		r_1
	(ii) $r_H < r_1$		r_H ($> r^{(e)}$)

TABLE 1. Classification of steady-solution branches. The quantities $r_2^{(e)}$, a_1^2, q_1 and q_2 are defined in the text by equations (3.8) and (5.2)–(5.4); for r_1 and r_H see §5. Types (*b*-ii), (*e*-ii) and (*g*-ii) are not illustrated in figure 2.

some of the more perplexing features of the full two-dimensional problem. In particular it provides strong evidence for the conjecture that the stable steady branches in figures 1 (*a*, *b*) are in fact connected to $r^{(e)}$ by an unstable steady branch, and that these results correspond to types (*e*) and (*f*) respectively.

5. Stability of the steady solutions: detailed considerations

In this section we amplify and justify some of the qualitative statements made in §4. We begin by giving a more precise classification of the three types of steady-solution branches.

From equation (4.3) it is easy to locate the turning points on the steady-solution branches. These satisfy the condition $dr/da^2 = 0$, and so occur when a^2 is a real, positive root of the cubic equation

$$f(a^2) \equiv a^6 + 3\mu a^4 + a^2[3\mu^2 - \mu q\{(4-\varpi) - (7-2\varpi)\mu\}] + [\mu^3 + \mu^2 q\{(2-\varpi) + \mu\}] = 0. \quad (5.1)$$

Since the sum of the roots of (5.1) is negative, there are at most two turning points. These coincide and form an inflection point at

$$a^2 = a_1^2 = \mu\left\{\frac{5-2\varpi-(2-\varpi)\mu}{4-\varpi-(7-2\varpi)\mu}\right\}, \quad (5.2)$$

when q has the value

$$q_1 = \frac{27\mu(1-\mu)^2(3-\varpi)^2}{[4-\varpi-(7-2\varpi)\mu]^3}, \quad (5.3)$$

provided only that $q_1 > 0$ and $a_1^2 > 0$. The type-(*c*) steady branch then obtains when $r_2^{(e)} \geqslant 0$ and either $a_1^2 < 0$, or $q_1 < 0$, or $0 < q < q_1$ and $a_1^2 > 0$. If $r_2^{(e)} \geqslant 0$, and $q > q_1 > 0$, $a_1^2 > 0$, then the type-(*b*) branch obtains. The first turning point occurs for some

$r > r^{(e)}$ (if $r_2^{(e)} < 0$, there is only one turning point and it is at some $r < r^{(e)}$, *cf.* type (*a*)). Then if

$$q > q_2 \equiv \frac{4\mu(3-\varpi)(1-\mu)}{[1-(4-\varpi)\mu]^2}, \tag{5.4}$$

the second turning point is at $r < r^{(e)}$, while if $q < q_2$ it is at $r > r^{(e)}$ and the steady solutions are all supercritical. Let r_1 be the value of r, at the sole turning point for types (*a*) and (*d*), or at the left-hand turning point for types (*b*), (*e*) and (*g*). Then the different types of steady solution branches are summarized in table 1 with reference to figure 2. We may note that cases (*b*), (*e*) and (*g*) do not arise in modelling the effects of solutes or rotation (Veronis 1965, 1966), where there are no nonlinear terms in the analogues of (2.17*a*).

The stability properties of the different types are obtained by linearizing equations (2.17) about the steady solutions (4.2) and (4.3), and looking for solutions that grow like $\exp s\tau$. The growth rate s is given by the roots of a quintic dispersion relation

$$s^5 + As^4 + Bs^3 + Cs^2 + Ds + E = 0, \tag{5.5}$$

where

$$A = 1+\varpi+\sigma+(5-\varpi)\zeta, \tag{5.6}$$

$$B = (\varpi+1)[(5-\varpi)\zeta+\sigma]+(5-\varpi)\zeta\sigma+\varpi(1+\mu+2a^2)-(1-c)\sigma r+\zeta q\alpha\sigma, \tag{5.7}$$

$$\begin{aligned} C = {} & \varpi\sigma(\mu+a^2)+\zeta q\beta\sigma+(\varpi+1)[\varpi(\mu+a^2)+(5-\varpi)\zeta\sigma+\zeta q\alpha\sigma] \\ & +\varpi(1+a^2)[(5-\varpi)\zeta+\sigma]-\varpi\sigma r(1-c-ab)-(5-\varpi)\zeta\sigma r(1-c), \end{aligned} \tag{5.8}$$

$$\begin{aligned} D = {} & (\varpi+1)\sigma[\varpi(\mu+a^2)+\zeta q\beta]+\varpi(1+a^2)[\varpi(\mu+a^2)+(5-\varpi)\zeta\sigma+\sigma\zeta q\alpha] \\ & -\varpi(5-\varpi)\zeta\sigma r(1-c-ab)-\varpi\sigma r(1-c)(\mu+a^2), \end{aligned} \tag{5.9}$$

$$E = \varpi\sigma(1+a^2)[\varpi(\mu+a^2)+\zeta q\beta]-\varpi^2\sigma r(1-c-ab)(\mu+a^2) \tag{5.10}$$

and

$$\alpha = \frac{\mu[(4-\varpi)^2a^2+\mu]}{(\mu+a^2)^2}, \quad \beta = \frac{(4-\varpi)^2\zeta[\zeta^2\{3(3-\varpi)a^2+\mu\}-\varpi a^4]}{\varpi(\mu+a^2)^2}. \tag{5.11}$$

Consider first the steady solutions that are marginally stable ($s = 0$). They are given by the solutions to the equation $E = 0$. In order to find the roots of this equation we substitute the steady solutions (4.2) into (5.10) and then use (4.3) and (5.11) to eliminate r and β in favour of a^2. After a fair amount of algebra, the condition $E = 0$ reduces to

$$a^2 f(a^2) = 0, \tag{5.12}$$

where the function $f(a^2)$ was defined in (5.1). The solution $a^2 = 0$ corresponds to the neutrally stable point $r^{(e)}$ already found for the static solution, while the condition $f(a^2) = 0$ defined the turning points where $dr/da^2 = 0$. Hence (5.12) states that, apart from $r^{(e)}$, the turning points are the only marginally stable points on the $a^2(r)$ curve, as claimed in §4. This result is in fact a general one (*cf.* Da Costa *et al.* 1981).

We next note that in the neighbourhood of $r^{(e)}$

$$E = 2\sigma\zeta^2\varpi(4-\varpi)r_2^{(e)}a^2 + O(a^4). \tag{5.13}$$

Since $-E$ is equal to the product of the eigenvalues of the quintic dispersion relation (5.5), we may use this result to say something about the small eigenvalue associated with the bifurcation (*cf.* §4). The bifurcation at $r^{(e)}$ is simple and so only one eigenvalue

changes sign, the other four remaining bounded away from zero with values close to those given by the two non-zero eigenvalues of (3.1) and those of the decoupled equations for c and e. The latter all have negative real parts if $\omega_0^2 < 0$, so that the small fifth eigenvalue (proportional to a^2) must be negative when $r_2^{(e)} > 0$ or positive when $r_2^{(e)} < 0$, in agreement with the general result quoted in §4. On the other hand, when $\omega_0^2 > 0$ ($r^{(o)} < r^{(e)}$) one of the non-zero eigenvalues at $r^{(e)}$ is positive (*cf.* §3), so that the product of the four large eigenvalues is negative. Hence the small eigenvalue arising from the proximity to the bifurcation is positive when $r_2^{(e)} > 0$, and negative when $r_2^{(e)} < 0$, in agreement with the general result.

We consider finally the points where $\mathscr{R}s = 0$, corresponding to the marginal overstability of the steady solution. Such points satisfy the condition

$$(E - AD)^2 = (BE - CD)(C - AB), \tag{5.14}$$

where the coefficients $A, \ldots, E$ are given by (5.6)–(5.10), provided that the corresponding oscillation frequency is real. At such points, where $r = r_H$, a branch of oscillatory solutions bifurcates from the steady-solution branch (a Hopf bifurcation). As before it is convenient to use equation (4.2) to eliminate r, and to solve the resulting expression for a^2. In general this cannot be done analytically and has to be done numerically. In the case $\omega_0^2 < 0$, we find that (5.14) always has a solution that falls between the two turning points (when they exist), or between $r_{\min}$ and $r^{(e)}$ when $r_2^{(e)} < 0$. However, this solution corresponds to the condition that there are two real and opposite eigenvalues s, and is not a Hopf bifurcation. On the other hand when $r(a^2)$ is monotonically increasing, there are in general no solutions except for a possible Hopf bifurcation at large values of a^2. This bifurcation is always present for sufficiently large values of σ and is of the same type as that present in the Lorenz (1963) equations, reducing to it in the limit $q \to 0$ for fixed ζ, $0 < \zeta \ll 1$. As discussed by Da Costa *et al.* (1981) the aperiodic behaviour found in the neighbourhood of this bifurcation and beyond is not physically significant in so far as it is not a feature of the solutions of the full two-dimensional problem. This is because it occurs at such large supercritical Rayleigh numbers that more modes would be expected to be excited than are retained in the truncation. Therefore we shall not dwell on this property of equations (2.17) any further.

On the other hand, when $\omega_0^2 > 0$ ($r^{(o)} < r^{(e)}$) and $r_2^{(e)} > 0$ the steady branch is doubly unstable in the neighbourhood of $r^{(e)}$. Then if the branch is monotonic a Hopf bifurcation must always be present if the steady solution is to gain stability at larger r (*cf.* §4). For smaller ζ the steady branch develops two turning points but σ can always be decreased sufficiently that $r^{(o)}$ is close to $r^{(e)}$ and the Hopf bifurcation occurs before the first turning point is reached. Such a solution, of type (g), is similar to those of type (f) in the neighbourhood of $r^{(e)}$. At the Hopf bifurcation there is a pair of complex eigenvalues with vanishing real part; the real part becomes negative beyond the bifurcation point, while the imaginary parts decrease again and vanish before the first turning point is reached. Between this point and the turning point these eigenvalues are real and negative; one of them passes through zero at the turning point, and remains positive until the second turning point. The portion of the steady branch between the bifurcation and the first turning point is therefore stable, while that between the two turning points is unstable. If σ is now increased, the Hopf bifurcation can either tend to a limiting position below the first turning point (*cf.* §7), or it can move up the steady branch and reach the turning point. The behaviour of the eigenvalues in the former case

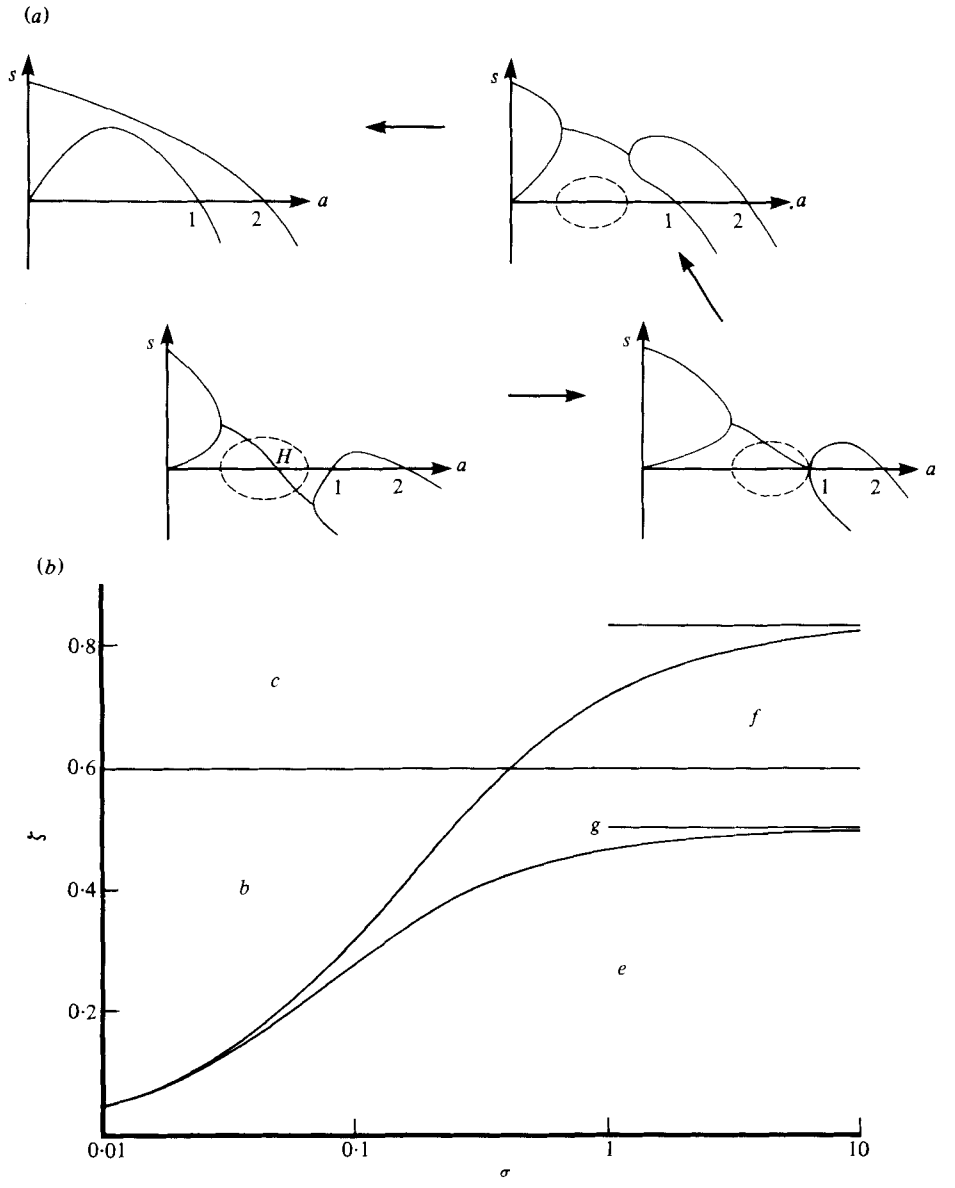

FIGURE 3. (*a*) The transition from type (*g*) to type (*e*) as σ is increased. Sketches showing the behaviour of the two relevant eigenvalues, as functions of a, along the steady branch. Solid lines show real parts of s, broken lines imaginary parts where s is complex. The Hopf bifurcation and the first and second turning points are indicated by H, 1, 2 respectively. (*b*) Different types of solution in the (σ, ζ)-plane for $q = 5$, $\varpi = 2$.

is as described above. In the latter case the magnitude of the imaginary eigenvalues at the Hopf bifurcation decreases as the turning point is approached. When the Hopf bifurcation occurs at the turning point the imaginary parts of the eigenvalues vanish: there are therefore two zero eigenvalues, as can be verified from (5.14).

For still larger σ these two eigenvalues are real and positive just before the turning point, and one passes through zero at the first turning point, followed by the other at the second turning point. Such a solution is of type (*e*). This behaviour of the eigen-

values as σ is increased is illustrated in figure 3(*a*). Figure 3(*b*) shows the occurrence of the various solution types in the (σ, ζ)-plane. The figure is drawn for $\varpi = 2{\cdot}0$ and $q = 5{\cdot}0$, but would be qualitatively similar for other values. We note that a type-(*g*) solution exists for all σ, and $\zeta < 0{\cdot}598$ but that the corresponding region of the (σ, ζ)-plane is insignificant unless $0{\cdot}4 < \zeta < 0{\cdot}598$, i.e. the steady branch is not too subcritical. As $\sigma \to \infty$, type-(*g*) solutions exist for $0{\cdot}5 < \zeta < 0{\cdot}598$; this situation corresponds to the case when the Hopf bifurcation tends to a limit and does not reach the first turning point. On the other hand, for $\zeta < 0{\cdot}5$ the Hopf bifurcation always reaches the first turning point as σ is increased and a type-(*e*) solution-results, as sketched in figure 3(*a*).

The above results justify the description of the stability of the steady-solution branches that was given in §4. Physically, the most relevant quantity is $r_{\min}$, the smallest value of r at which *stable* steady convection is possible. This is obtained as a straightforward consequence of the stability discussion in §4, and the results for each branch type are summarized in table 1. We note finally that as $r_2^{(e)}$ decreases to zero so does the oscillation frequency associated with the Hopf bifurcation, and for $r_2^{(e)} < 0$ the condition (5.14) for a Hopf bifurcation gives instead the points with equal and opposite real eigenvalues. This provides the connection between the supercritical branch and the subcritical branch discussed earlier in this section.

6. Time-dependent solutions: subcritical convection

Except in the neighbourhood of $r^{(o)}$, finite-amplitude oscillatory solutions cannot be followed analytically. To investigate time-dependent behaviour we have therefore integrated the equations (2.17) numerically, using a standard NAGLIB routine based on a fourth-order Runge–Kutta–Merson scheme with variable time steps, chosen to ensure sufficient accuracy. These numerical results enable us to study changes in the form of the oscillations as r is increased above $r^{(o)}$ and to discover how the transition from the oscillatory to the steady branch takes place.

Oscillations exist for some range of r whenever $q > q_0 > 0$. Since the steady solutions do not depend on the Prandtl number σ, it follows from (3.6) that for any $q > \zeta/(1-\zeta)$ oscillatory solutions can be obtained, without affecting the basic character of the steady solutions, simply by increasing σ to sufficiently large values (*cf.* figure 3*b*). In this section we shall consider only cases where the steady branch allows subcritical convection, with $r_{\min} < r^{(e)}$, as in figures 2(*d*) or (*e*); the case when steady solutions are all supercritical, with $r_{\min} > r^{(e)}$, as for instance in figure 2(*f*), will be discussed in §7.

Table 2 lists the choices of parameters for the various cases that we have investigated. Figure 4(*a*) shows $a(r)$ on the steady branch for case *A*; since the figure is symmetrical about $a = 0$, only the positive branch is displayed. Oscillatory solutions can be represented by the maximum amplitude, $a_{\max}$, of a or by its root-mean-square value, both of which are plotted in the figure. For this case the oscillatory branch bifurcates supercritically from the static solution and oscillatory solutions exist for $r^{(o)} < r \leqslant r_c \simeq 3{\cdot}4059 < r^{(e)}$. (The exact value of r_c is sensitive to the accuracy of the numerical procedure. Both Runge–Kutta and predictor–corrector methods yield similar results, though r_c is marginally higher for the latter. With a cruder difference scheme, r_c was underestimated by about 2 %.)

Case	Type	q	ϖ	ζ	σ	λ	Q
A	*e*	2·5	2	0·4	1	1	98·7
B	*e*	5	2	0·4	1	1	197·3
C	*f*	5	2	0·67	10	1	197·3
D	*f*	15	0·8	0·5	1	$\frac{1}{2}$	3713
E	*fg*	5	2	0·598	10	1	197·3
F	*e*	5	2	0·4	10	1	197·3

TABLE 2. Parameters for cases treated in this paper.

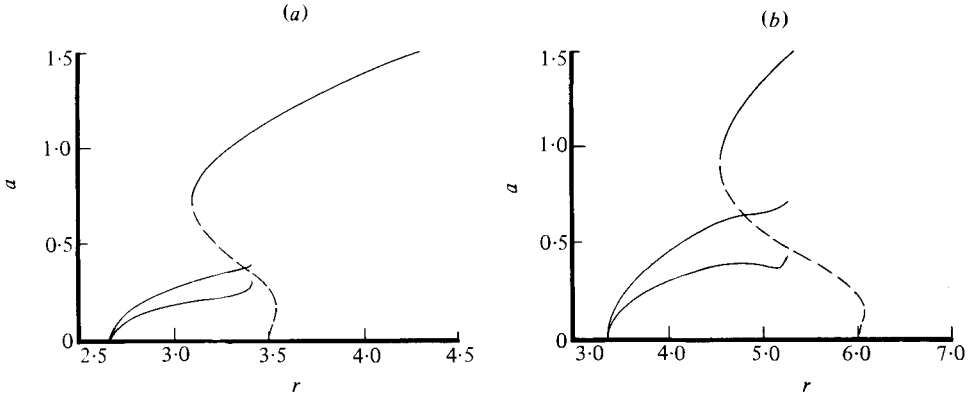

FIGURE 4. Subcritical convection: the steady and oscillatory branches. (*a*) Case *A*, (*b*) Case *B*. Both $a_{\max}$ and the r.m.s. value of a are shown on the oscillatory branch; the broken curve indicates the unstable portion of the steady branch.

For $r_{\min} < r < r_c$ both stable oscillatory solutions and stable steady solutions coexist, so that hysteresis can occur. The solution that is attained depends on the initial conditions. In general the domain of attraction of the oscillatory solution is smaller than that of the stable steady solution: a sufficiently large perturbation produces a transition from the oscillatory to the stable steady branch. However, if r is increased sufficiently gradually the oscillatory branch can be followed all the way to r_c, where the solution jumps to the stable steady branch. For $r > r_c$ only steady solutions can be reached. If r is then decreased through r_c the solution remains on the upper steady branch until $r = r_{\min}$, when it drops to the oscillatory branch.

The oscillations retain the symmetry of equations (2.17), for they are invariant under the transformation in which a, b and d change sign while c and e are unaffected. Consequently, if a, b and d vary with a period P then c and e have a period $\frac{1}{2}P$. The form of the oscillations undergoes a gradual change as r is increased from $r^{(o)}$ to r_c. Close to $r^{(o)}$, $a(\tau)$, $b(\tau)$ and $d(\tau)$ are small amplitude, nearly sinusoidal oscillations. As r is increased, the amplitude grows and the oscillations become more obviously nonlinear. Figure 5(*a*) shows a set of typical solutions, as functions of time, for $r = 3{\cdot}1$. In this and subsequent figures only the velocity a and the magnetic fluctuations d and e are plotted; the temperature, given by b and c, is usually less informative and behaves as in the double-diffusive problem discussed by Da Costa *et al.* (1981). In addition, the limit cycle is shown in the $(a, \dot{a})$-phase plane. The solutions, like relaxation oscillations, show rapid rises in amplitude, followed by more gradual falls, though c has the

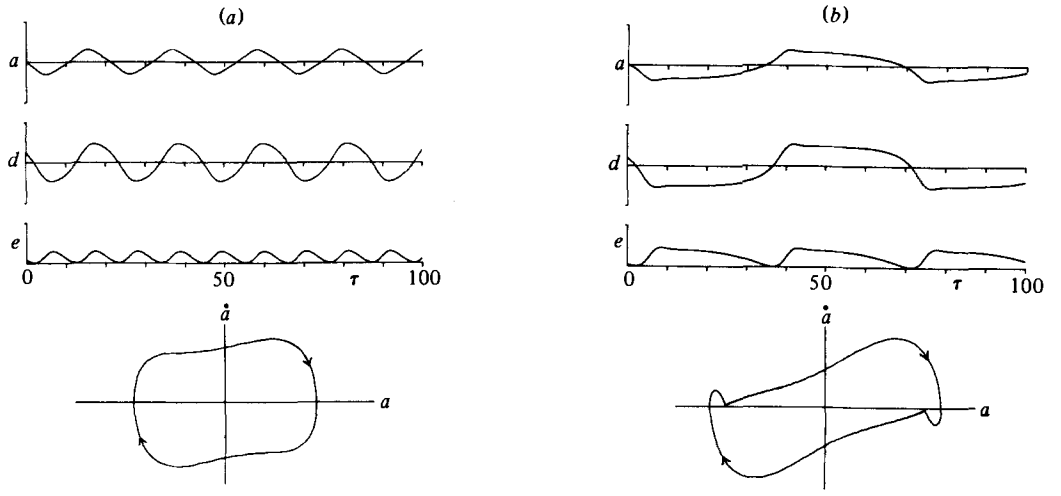

FIGURE 5. Oscillatory solutions for case A with (*a*) $r = 3{\cdot}1$, (*b*) $r = 3{\cdot}4$. For the three profiles of $a(\tau)$, $d(\tau)$, $e(\tau)$, the positive and negative ordinate axes are of unit length. The limit cycles are depicted in the $(a, \dot{a})$-plane, and the axes are of unit length.

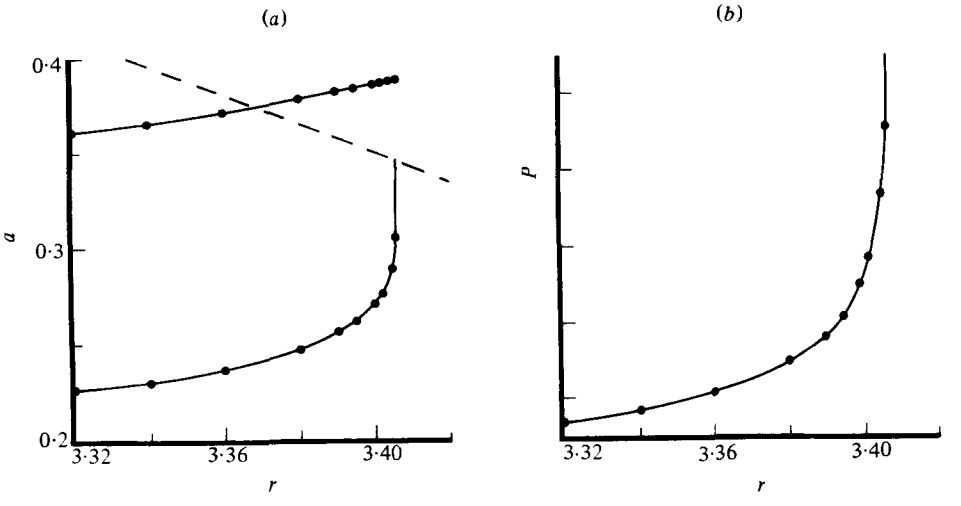

FIGURE 6. Termination of the oscillatory branch. (*a*) The maximum amplitude $a_{\max}$ and the root-mean-square amplitude, together with the unstable steady branch (broken line) as functions of r. (*b*) The period P of oscillatory solutions plotted against r. P tends to infinity and the r.m.s. value approaches the steady branch but $a_{\max}$ changes only slightly.

opposite behaviour. As expected, the period of e is seen to be half that of a and d. If r is increased still further the slow phase of the cycle lasts longer and the waveform becomes progressively flatter beyond each maximum. The resulting plateau is apparent in the set of solutions for $r = 3{\cdot}4$, just short of r_c, which is shown in figure 5(*b*), and the duration of this plateau increases rapidly as r tends to r_c. At the same time, a spike develops, corresponding to an initial overshoot, and this produces small lobes in the limit cycle of figure 5(*b*).

From figure 4(*a*) it appears that the oscillatory branch terminates on the unstable steady branch at $r = r_c$. In order to establish the nature of this transition we have

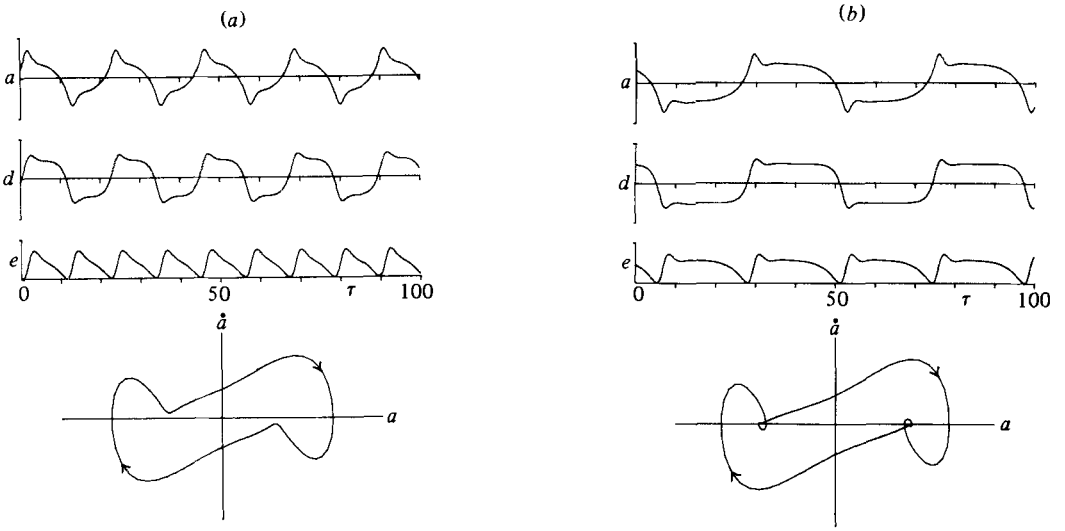

FIGURE 7. As figure 5 but for case B with (*a*) $r = 5{\cdot}2$, (*b*) $r = 5{\cdot}255$.

plotted in figure 6(*a*) an enlargement of the relevant part of figure 4(*a*), while figure 6(*b*) shows the period of the oscillations as a function of r, in the neighbourhood of r_c. The maximum amplitude changes slowly but the period begins to increase rapidly and tends to infinity as r approaches r_c. In this limit, the plateau of figure 5(*b*) extends forever, to give a steady solution; the steady solution is, however, unstable and so a snaps through to the upper branch. The development of the solutions in the vicinity of r_c can be represented by phase portraits in the $(a, \dot{a})$-plane, as for the analogous problem of thermosolutal convection (see figure 4 of Da Costa *et al.* 1981). For $r < r_c$ there is either an unstable focus or an unstable node at the origin, surrounded by a periodic orbit like the limit cycle in figure 5(*b*); beyond the symmetrical limit cycle lie a pair of saddle points and then a pair of stable nodes (corresponding to the unstable and stable steady solutions respectively). At $r = r_c$ the two saddle points are linked by a heteroclinic limit cycle of infinite period, and beyond r_c the limit cycle disappears. This pattern of behaviour has obvious resemblances to the finite-amplitude motion of a simple pendulum; there is, in fact, a limited range of parameters for which $a(\tau)$ is proportional to the Jacobian elliptic function $\mathrm{sn}(\tau^*)$, $\tau^* \propto \tau$ (Knobloch & Proctor 1981).

The amplitudes of the steady and oscillatory branches for case B are displayed in figure 4(*b*). This time the oscillations are more vigorous and more strikingly nonlinear. The solutions for $r = 5{\cdot}2$, shown in figure 7(*a*), are more spiky in appearance than those in figure 5. As r is increased, the spike becomes more pronounced and is followed by a flat shoulder, which develops into a plateau as $r \to r_c$. The limit cycle for $r = 5{\cdot}2$ has distinctive lobes, which are even more pronounced when $r = 5{\cdot}255$. In figure 7(*b*), a rises to a maximum, then drops down and overshoots the level of the shoulder; in the phase diagram this appears as a loop around the neighbourhood of the saddle point. Once again, the oscillatory branch terminates on the lower, unstable steady branch as the period becomes infinite, at $r = r_c \approx 5{\cdot}2558$. Since the maximum value of a reflects the height of the spike, $a_{\max}$ ends up well above the steady branch, as can be seen from figure 4(*b*). The r.m.s. value of a provides a better estimate, which

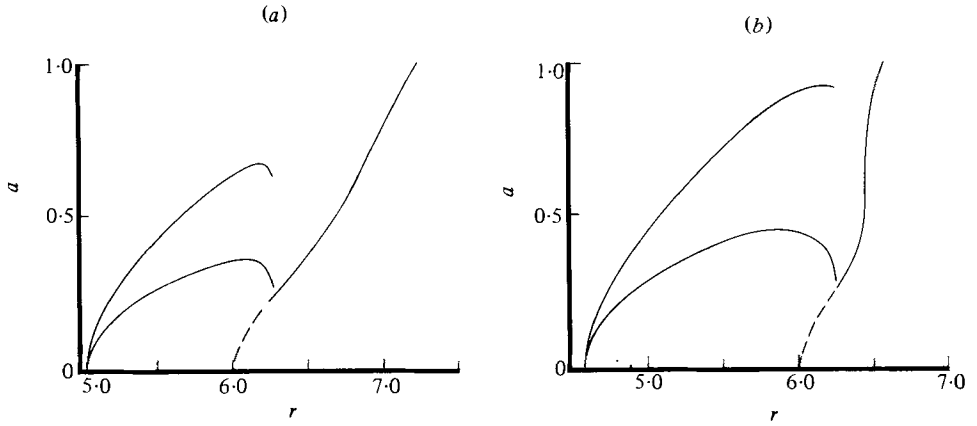

FIGURE 8. Supercritical convection. As figure 4 but (*a*) for case *C* and (*b*) for case *D*, with a point of inflection on the steady branch.

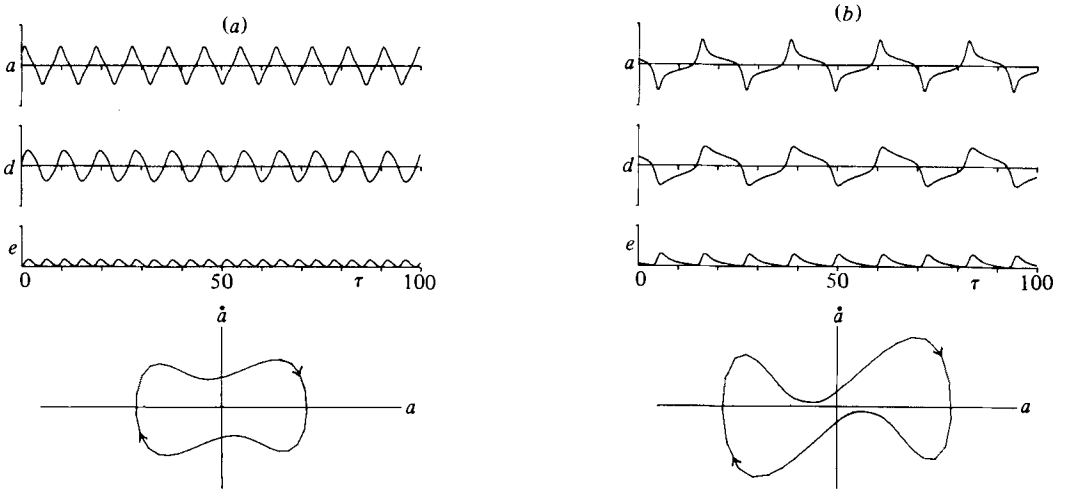

FIGURE 9. As figure 5 but for case *C* with (*a*) $r = 5{\cdot}6$, (*b*) $r = 6{\cdot}265$.

approaches the steady branch as $r \to r_c$. Nevertheless, in figure 4(*b*) as in figure 6(*a*), it is only at the last moment that the period becomes very large and the r.m.s. value swings upwards to join the unstable steady branch.

7. Time-dependent solutions: supercritical convection

The form of the steady branch can be altered by varying ζ while q and ϖ are held fixed. If q and ϖ retain the values for case *B*, while ζ is increased, $r_{\min}$ also increases until it becomes greater than $r^{(e)}$. The two turning points approach each other until they eventually coalesce at a point of inflection. From (5.3), this occurs when $q_1(\zeta) = q$ so that $\zeta \simeq 0{\cdot}598$. For larger values of ζ, r increases monotonically with a^2 on the steady branch but $r^{(o)} < r^{(e)}$ for $\zeta < 0{\cdot}82$. Figure 8(*a*) shows the steady and oscillatory branches for case *C*. As we saw in §4, the steady solution is stable only for $r > r_H > r^{(e)}$ and there is a Hopf bifurcation at $r_H \simeq 6{\cdot}2414$. For $r^{(e)} < r < r_H$ the pair

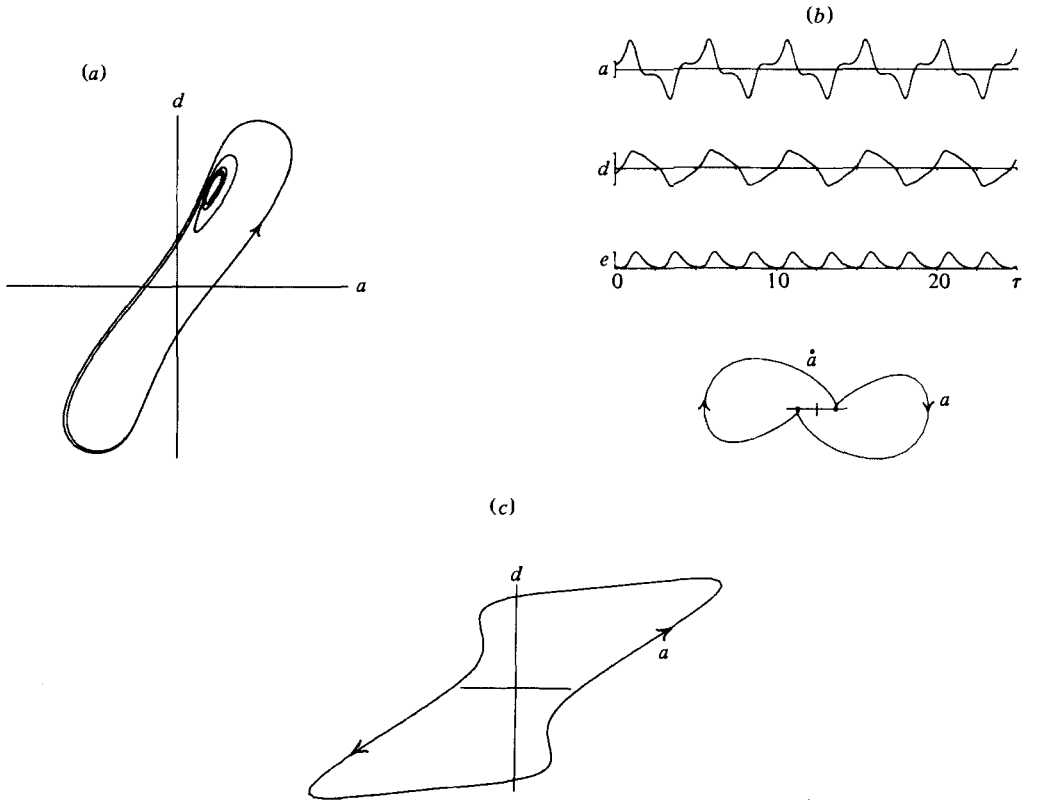

FIGURE 10. (a) Trajectory projected onto the (a, d)-plane for case C with $r = 6{\cdot}237$: the solution spirals out from the unstable fixed point to the limit cycle. The axes are of unit length. (b) As figure 5 but for case D with $r = 30$. (c) Limit cycle for case D with $r = 30$, projected onto the (a, d)-plane.

of saddle points (which corresponded to the unstable steady solution) is replaced by a pair of unstable nodes or foci and the oscillatory branch no longer joins the steady branch as the period of the oscillation becomes infinite. The numerical solutions do, however, make it possible to describe the connection between the two branches.

As r is increased from $r^{(0)}$, $a_{\max}$ increases monotonically and reaches a maximum when $r \simeq 6{\cdot}25$. Thereafter, $a_{\max}$ falls by about 6 % until, at $r \simeq 6{\cdot}270$, the oscillatory branch disappears and solutions spiral in towards the stable steady branch. The form of the oscillatory solutions changes as r is increased and differs from the cases that have already been displayed. Figure 9 shows solutions for $r = 5{\cdot}6$, which are almost symmetrical about the peaks, and for $r = 6{\cdot}265$, the highest value for which such oscillations could be found. The spikes of figure 7 (a) are still present but $|a|$ decreases gradually after the peaks and there are no plateaux in $d(\tau)$. The corresponding limit cycle resembles a horizontal figure-of-eight.

For r slightly greater than r_H there are transient oscillations which gradually decay; for r slightly less than r_H the solutions spiral slowly outward from the unstable focus and ultimately develop into large-scale oscillations. Figure 10 (a) shows such a solution, projected onto the (a, d) phase plane. After spiralling many times around the unstable fixed point, the trajectory settles down to a limit cycle, whose shape is

characteristic of cases A, B and C. The behaviour of solutions in the neighbourhood of r_H implies that the Hopf bifurcation is subcritical. We conjecture that the (unstable) small-amplitude oscillations about the stable steady solution, for r slightly greater than r_H, are connected to the large-amplitude oscillations by an unstable oscillatory branch, as sketched in figure 2(f). This branch links asymmetrical to symmetrical trajectories. We have not attempted to compute these unstable oscillatory solutions but strong evidence for this conjecture is provided by Knobloch & Proctor (1981). They found analytically that there was such an unstable oscillatory branch in the limit $r^{(e)} - r^{(o)} \ll r^{(e)}$, and showed that the transition between large-amplitude, zero mean oscillations and small-amplitude oscillations with non-zero mean occurs *via* an unstable ambiclinic limit cycle of infinite period. Moreover, in the large-amplitude oscillations they found that $a(\tau)$ was proportional to the Jacobian elliptic function $\mathrm{cn}\,(\tau^*)$, which is consistent with the behaviour in figure 10(b).

All the cases considered so far correspond to square cells ($\lambda = 1$, $\varpi = 2$). When $\lambda < 1$ it follows from (3.8) that $r_2^{(e)}$ is large and positive, provided ζ is sufficiently small. Thus narrow cells, which are favoured by linear theory, are more likely to have solutions of type (f). Case D has $\lambda = \frac{1}{2}$ and a relatively large value of q. As a result, $r_{\min}$ is distinctly greater than $r^{(e)}$ ($r_{\min} = r_H \simeq 26{\cdot}7$, $r^{(e)} = 16$). The character of the large-amplitude oscillations, shown in figure 10(b) for $r = 30$, differs from that in figure 9. The spike in $a(\tau)$ remains but now it is preceded, and not followed, by a shoulder. The corresponding limit cycle in the $(a, \dot{a})$-plane is quite different from that in figure 9(b), just as the limit cycle in the (a, d)-plane, shown in figure 10(c), differs from that in figure 10(a). This pattern of behaviour is similar to that found for the full two-dimensional problem in figure 1(d) (see also Weiss 1981c).

When $\zeta \simeq 0{\cdot}598$ there is a point of inflection on the steady branch. This is the critical case separating solutions of type (f) from those of type (g). For $0{\cdot}598 < \zeta < 0{\cdot}82$, there is a Hopf bifurcation on the steady branch as we have just seen; for ζ slightly less than 0·598 there are two turning points, with a Hopf bifurcation below the first turning point, and the steady solution is stable between the Hopf bifurcation and that turning point, as predicted in §4. However, the connection between the large-scale oscillations and the Hopf bifurcation differs from that described above for case C. We shall describe this new pattern of behaviour for case E, with $\zeta = 0{\cdot}598$.

The oscillatory and steady branches for this case are shown in figure 8(b); the Hopf bifurcation occurs for $r = r_H \simeq 6{\cdot}263$ and lies below the inflection point. For $r < 6{\cdot}22$ the oscillatory solutions resemble those displayed in figure 9(b), for case C, and the corresponding limit cycle in the (a, d)-plane is similar to that eventually attained in figure 10(a). When $r = 6{\cdot}23$ the solution hovers about the unstable fixed points before proceeding on its way and when $r = 6{\cdot}24$ the trajectory circles once about each fixed point, as shown in figure 11(a), projected on to the (a, d)-plane. The limit cycle for $r = 6{\cdot}25$ is shown in figure 11(b): now the trajectory circles twice about each fixed point, as shown in detail in figure 11(c). As $r \to r_H$ the limit cycle remains symmetrical but the number of spirals about the fixed points increases. Figure 11(d) shows a detail of the trajectory for $r = 6{\cdot}26$, with 8 spirals about the fixed point. Apparently the limit cycle approaches the fixed point along its stable manifold and is then thrown out on the unstable manifold. For $r = 6{\cdot}263$, the numerical solutions still spiral slowly outwards but for $r = 6{\cdot}264$ they gradually spiral in to a fixed point, so confirming that the steady solution is stable for $r > r_{\min} = r_H$. In case C the oscillatory branch became

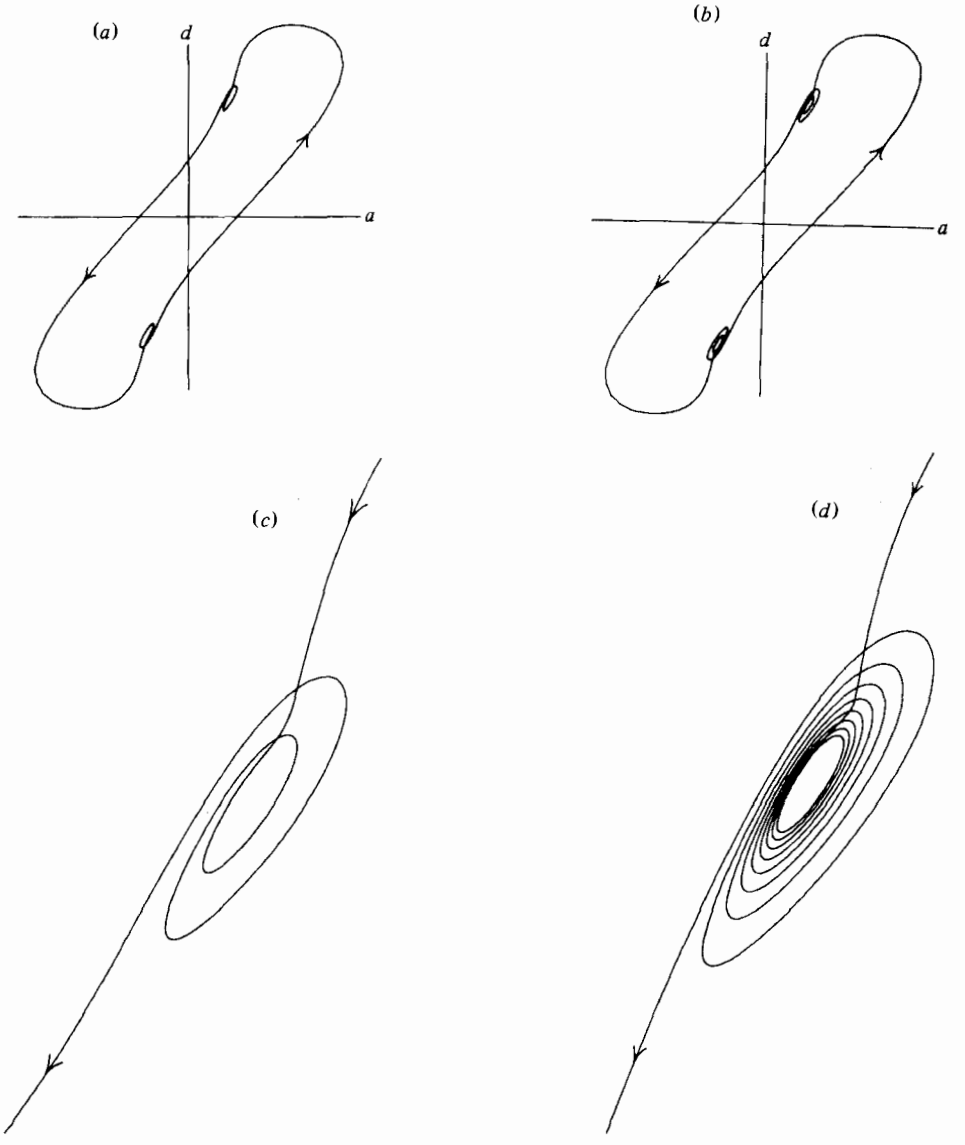

FIGURE 11. Limit cycles for case E, projected onto the (a, d)-plane. Trajectories: (a) for $r = 6{\cdot}24$ with one loop about each fixed point, (b) for $r = 6{\cdot}25$, with two loops; (c) shows a detail of (b), and (d) shows a detail for $r = 6{\cdot}26$, with eight loops.

unstable while the period was finite; here the oscillatory branch apparently terminates on the steady branch as the period becomes infinite. As $r \to r_H$ the variables $a(\tau)$ etc. vacillate almost indefinitely about their values for the unstable steady solution. The bifurcation at r_H is probably subcritical but it is not a standard Hopf bifurcation. The behaviour depicted in figure 11 is possible because (2.17) is a fifth-order system, whose solutions necessarily cannot be adequately represented on a two-dimensional phase plane. There are indications of similar behaviour in the full two-dimensional problem, where some solutions vacillate about a steady state before abruptly reversing the direction of motion (Weiss 1981*c*); these solutions are not, however, periodic.

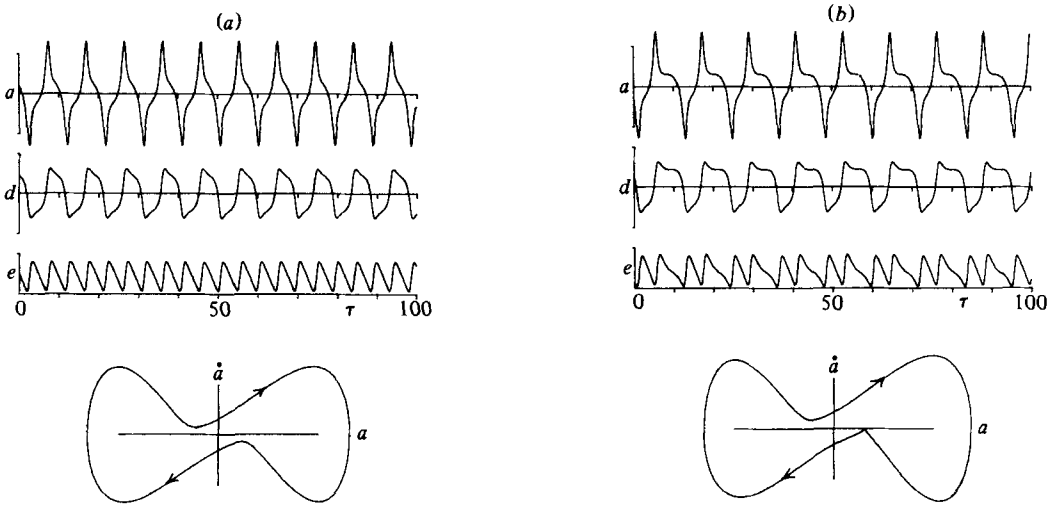

FIGURE 12. As figure 5 but for case F with (*a*) $r = 5{\cdot}20$ (symmetrical limit cycle) and (*b*) $r = 5{\cdot}25$ (asymmetrical limit cycle, with a single cusp).

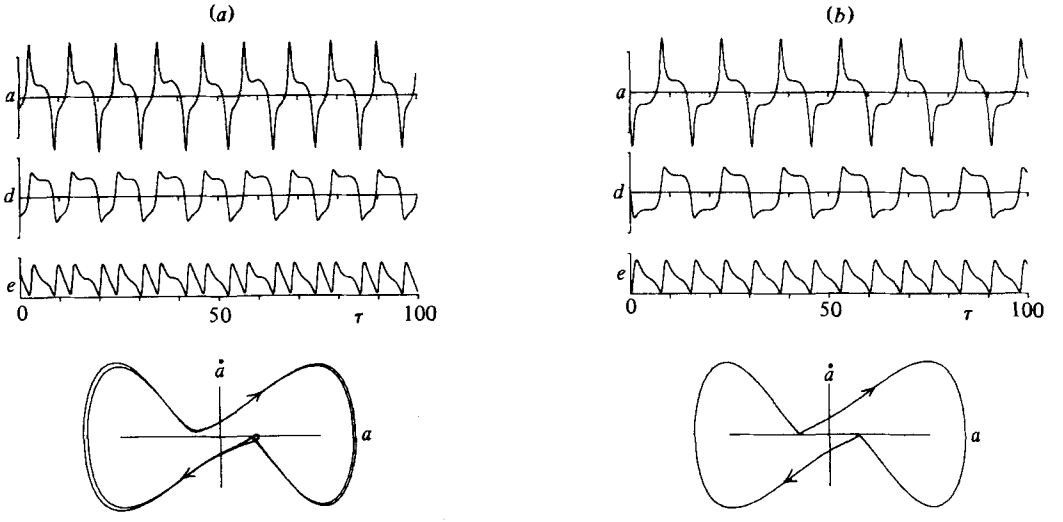

FIGURE 13. As figure 5 but for case F with (*a*) $r = 5{\cdot}28$ (period doubled) and (*b*) $r = 5{\cdot}33$ (symmetrical limit cycle with two cusps).

8. Bifurcations from the oscillatory solutions

The oscillations described in § 6 were all symmetrical about the static solution, and the loops shown in figure 11 developed symmetrically about the two fixed points. Numerical solutions for the full two-dimensional problem show that there may also be a bifurcation from symmetrical to asymmetrical oscillations (Weiss 1981*a*). Moreover, in the related problem of thermosolutal convection there is, in certain circumstances, a similar bifurcation, which is followed by a sequence of bifurcations at each of which the period doubles, until the solutions become aperiodic (Da Costa *et al.* 1981). Similar patterns of behaviour have been found in other nonlinear systems and it is natural to expect them here.

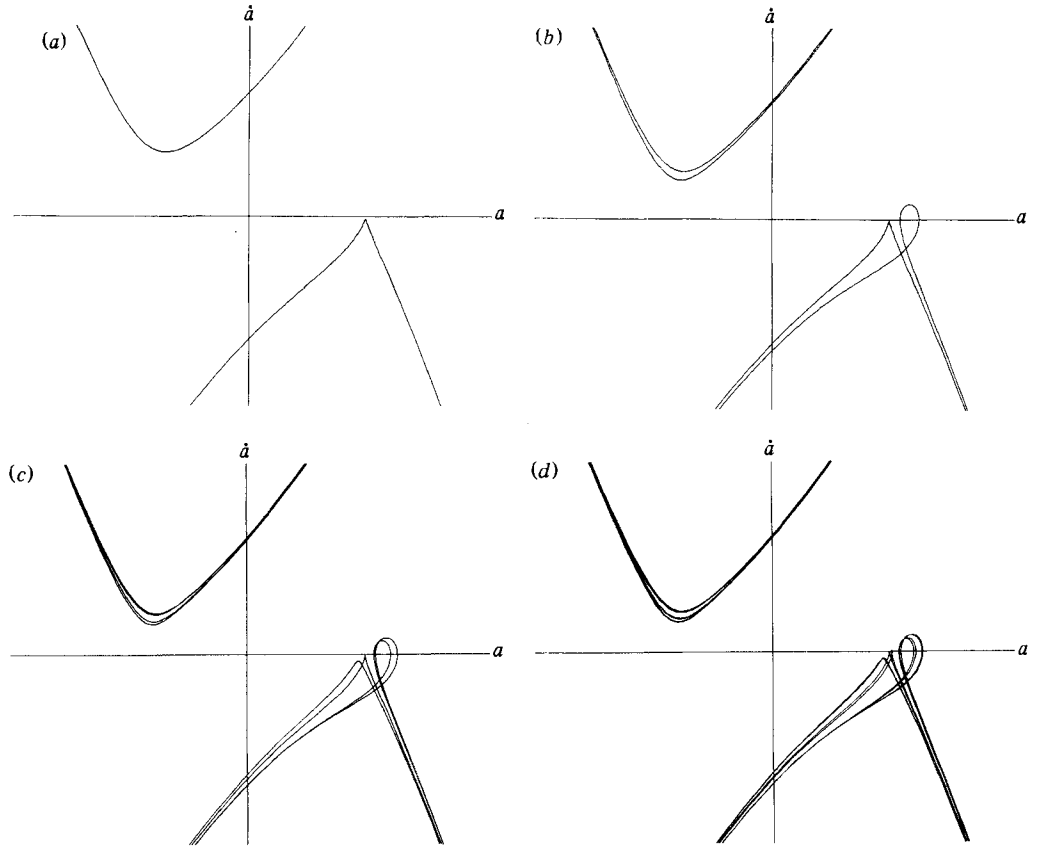

FIGURE 14. Details of limit cycles in the $(a, \dot{a})$-plane for case F with (*a*) $r = 5{\cdot}250$ (asymmetrical, *cf.* figure 12*b*), (*b*) $r = 5{\cdot}280$ (period doubled, *cf.* figure 13*a*), (*c*) $r = 5{\cdot}288$ (period quadrupled) and (*d*) $r = 5{\cdot}289$ (period octupled).

Such bifurcations do appear in case F, which is of type (*e*) and similar to case B. The maximum amplitude of the oscillation rises well above the unstable steady branch and solutions for $r = 5{\cdot}20$ are shown in figure 12(*a*). These solutions are symmetrical and resemble those in figure 9(*b*). In particular, a and d have a period P while e has a period $\frac{1}{2}P$. The results for $r = 5{\cdot}25$, in figure 12(*b*), show that a bifurcation has occurred. The limit cycle has a cusp for $a > 0$, which is not present for $a < 0$ and corresponds to the shoulders that follow maxima in $a(\tau)$; $e(\tau)$ appears irregular and its period has increased to P. There is, of course, another asymmetrical solution which can be obtained by transforming a to $-a$ etc.

This bifurcation to asymmetry is followed by further bifurcations at which the period doubles. In figure 13(*a*), for $r = 5{\cdot}28$, successive cycles are no longer identical: alternate shoulders in $a(\tau)$ have a subsidiary peak, while every fourth peak in $e(\tau)$ is followed by a flat shoulder. The limit cycle shows that a loop has separated from the cusp, as shown in greater detail in figure 14. At $r = 5{\cdot}288$, the cusp and loop have each split and the period has quadrupled. (The corresponding differences in $a(\tau)$ are just visible to the eye of faith.) By $r = 5{\cdot}289$, after a further bifurcation, the period has octupled: details of the limit cycle are displayed in figure 14. At $r = 5{\cdot}29$ the solution

seems to be aperiodic. Cusps alternate with loops but successive pairs of cycles differ slightly and the solution never repeats itself exactly. These results are consistent with the occurrence of a Feigenbaum sequence of bifurcations, in which the increments in r between successive bifurcations decrease in a geometric progression, with chaotic behaviour beyond the accumulation point (Feigenbaum 1978; Franceschini & Tebaldi 1979; Franceschini 1980). The existence of apparently aperiodic solutions over a finite range of r suggests that a strange attractor has appeared.

When r is increased further, the solution remains chaotic for $r = 5{\cdot}30$. But for $r = 5{\cdot}31$ the oscillation is quadruply periodic and for $r = 5{\cdot}315$ there is an asymmetrical solution resembling that in figure 12(*b*). So chaos is followed by an inverse sequence of bifurcations at each of which the period is halved. Thereafter the solutions become more symmetrical. The results for $r = 5{\cdot}325$ show that there has been a further bifurcation: the solutions in figure 13(*b*) are symmetrical but unlike those in figure 12(*a*) there are two distinct cusps, which become more pronounced as r is increased. When $r = 5{\cdot}333$ the cusps have developed into small loops and by $r = 5{\cdot}334$ the oscillatory branch has lost stability.

Period-doubling was also found when the equations were solved using a predictor–corrector scheme, though the bifurcation points were slightly different. On the other hand, no bifurcations were detected with a less accurate Runge–Kutta method. Further work is needed to establish the nature of the bifurcations and to determine whether they are relevant to the full two-dimensional problem. In any case, fine details (like those in figure 14) would probably be masked by the effects of truncation errors and slowly decaying transients in any two-dimensional computation.

9. Conclusion

The results that we have presented provide a fairly complete description of the principal features exhibited by solutions of the model problem. Steady solutions may be either subcritical or supercritical, and their stability is affected by the presence of an oscillatory branch. That branch may terminate in various ways: by joining the unstable steady branch as the period goes infinite, by connecting to a Hopf bifurcation on the supercritical steady branch or, more exotically, by a bifurcation to asymmetrical oscillations, followed by a sequence of bifurcations leading to the possible appearance of a strange attractor. These features of solutions of equations (2.17) correspond closely to the behaviour of solutions of the full two-dimensional equations (2.5) (Weiss 1981*a*, *b*, *c*).

The full problem, like the model problem, allows subcritical solutions, like that in figure 1(*a*), though the magnitude of $r^{(e)} - r_{\min}$ is exaggerated in the truncated system. With different choices of parameters, as in figure 1(*c*, *d*), only supercritical steady solutions are obtained, with Hopf bifurcations like those found in cases *D* and *E*. The oscillatory solutions are more complicated than those discussed here and also more difficult to compute. Typically, the maximum amplitude rises to a maximum and then falls off until the oscillatory branch comes to an end. At the same time the oscillations become spasmodic, like those in figure 9(*b*), and their period increases. In certain cases, the oscillations became strongly asymmetrical shortly before they disappeared.

For fixed values of the physical parameters (magnetic field strength and diffusivities)

		$R_{\min}$				
λ	$R^{(e)}$	$\zeta = 0{\cdot}4$	$\zeta = 0{\cdot}2$	$\zeta = 0{\cdot}1$	$\zeta = 0{\cdot}01$	$\zeta = 0{\cdot}001$
5	$2{\cdot}54 \times 10^6$	10607	6005	4208	2871	2752
4	$1{\cdot}66 \times 10^6$	11263	5560	3466	2007	1883
3	$9{\cdot}76 \times 10^5$	13937	5826	3079	1351	1217
2	$4{\cdot}88 \times 10^5$	23107	8083	3454	943	778
$\sqrt{2}$	$2{\cdot}93 \times 10^5$	40352	12904	4858	903	680
1	$1{\cdot}96 \times 10^5$	75079	23075	8123	1167	814

TABLE 3. Subcritical and supercritical convection ($Q/\pi^2 = 1000$).

the form of the steady branch, both in the full problem and in our truncated system, depends critically on the cell width λ. For instance, case *B*, with $Q = 200$ and $\lambda = 1$, has a subcritical steady branch (*cf.* figure 3*b*) but for the same values of Q and ζ a narrower cell, with $\lambda = \frac{1}{2}$, has a steady branch on which $r(a^2)$ is a monotonically increasing function. In this example $R^{(e)}$, the Rayleigh number at the simple bifurcation, is in any case slightly less for $\lambda = 1$ than for $\lambda = \frac{1}{2}$ but, for large Q, $R^{(e)}$ is least when $\lambda \simeq (Q/2\pi^2)^{-\frac{1}{4}} \ll 1$. Thus linear theory favours narrow cells. In practice we want to find the lowest value of the temperature gradient for which steady convection can occur; thus we need to calculate $R_{\min}$, the lowest value of R for which steady convection is possible, and then to find the value of λ (which may be of order unity) for which $R_{\min}$ is least. This can only be done if nonlinear solutions are available.

To illustrate this, we consider a particular case, with $Q/\pi^2 = 1000$. Then $R^{(e)}$ is least for $\lambda \simeq 0{\cdot}37$, when $R^{(e)} \simeq 118400$, and $R^{(e)}$ becomes very large for λ of order unity, as can be seen from table 3. For the model equations $R_{\min}$ can easily be found from (4.3) and table 3 gives values of $R_{\min}$ for various choices of ζ and λ. When $\zeta = 0{\cdot}4$, $R_{\min}$ is least for $\lambda \simeq 5$ and is then much less than $R^{(e)}$; moreover, for $\lambda < 0{\cdot}7$ the steady branch becomes supercritical and so (for sufficiently large σ) $R_{\min} > R^{(e)}$. As ζ is reduced, the value of λ for which $R_{\min}$ is least becomes smaller but remains of order unity. More generally, if $Q \gg 1$, $\zeta \ll 1$ we can consider two extreme cases. For $\zeta^2 \ll \zeta^2 q \ll a^2 \ll 1$ it follows from (4.3) that $r \simeq 1$ and so $R_{\min}$ has the same value as the critical Rayleigh number in the absence of a magnetic field, which is least when $\lambda = \sqrt{2}$. For $\zeta^2 q \gg 1$, $R_{\min}$ is least when $\lambda^4 = 4\zeta^2 q$. In the former case, the lowest value of $R_{\min}$ is $6{\cdot}75\pi^4$, in the latter it is $8\pi^3 \zeta Q^{\frac{1}{2}}$, in agreement with the results in table 3.

Thus steady convection first appears with λ of order unity, or greater, and the nonlinear results are quite different from the predictions of linear theory. This is a feature of solutions to the full two-dimensional equations also (Weiss 1981*b*), though $R_{\min}$ is larger than it is for the truncated system. When higher-order terms are included in the representation of the flux function A, Busse (1975) has shown that, for $\lambda = 1$,

$$R_{\min} = 8\pi^4 + \tfrac{5}{2}(17{\cdot}25\pi\zeta^{\frac{1}{2}}Q)^{\frac{4}{5}}, \tag{9.1}$$

provided that $\zeta^{\frac{1}{2}}Q \ll 1 \ll Q/\zeta^2$, and this result is confirmed by numerical experiments for $\zeta^{\frac{1}{2}}Q \lesssim 100$.

In astrophysical applications it is important to be able to estimate the value of the superadiabatic temperature gradient at which steady convection first occurs, as well as the scale of the resulting motion. As we have seen, this can only be done on the

basis of nonlinear calculations. The simplified model that we have presented here reflects the richness of the full problem and provides a reliable guide to the behaviour of its numerical solutions. Moreover, it serves as a paradigm for other double-diffusive systems.

This investigation was stimulated by the GFD program at Woods Hole Oceanographic Institution and we have benefited from discussions with J. Guckenheimer, L. N. Howard, A. M. Soward, C. T. Sparrow, E. A. Spiegel and P. Swinnerton-Dyer. We are grateful to Dr C. T. Sparrow for making his program for solving ordinary differential equations available to us and to Dr J. M. Wheeler for assistance in carrying out the computations. Much of this work was carried out at the Harvard–Smithsonian Center for Astrophysics; E.K. acknowledges support from the Harvard Society of Fellows and St. John's College, Cambridge, N.O.W. from the Langley–Abbot Program of the Smithsonian Institution and L.N. Da C. from NSF grant AST 77-25656.

Appendix. Finite-amplitude oscillatory modes

Modified perturbation theory may be employed to investigate oscillatory solutions in the neighbourhood of the Hopf bifurcation at $r^{(o)}$. The treatment applies both to the full system (2.5) and to the truncated system (2.17). However, equations (2.17) suggest a procedure that is more economical than the methods that have been used for related problems (Veronis 1959; Huppert & Moore 1976). Since this procedure can also be applied in other contexts, we provide an outline of it here.

We start by substituting from the expansion (3.9) into the equations (2.17), and then equate the coefficients of successive powers of ϵ. To zeroth order in ϵ the equations are identically satisfied and in first order we obtain the condition

$$\mathbf{L}_0 \begin{pmatrix} a_1 \\ b_1 \\ d_1 \end{pmatrix} = \begin{pmatrix} i\omega_0+\sigma & -\sigma r^{(o)} & \sigma\zeta q \\ -1 & i\omega_0+1 & 0 \\ 0 & -1 & i\omega_0+\zeta \end{pmatrix} \begin{pmatrix} a_1 \\ b_1 \\ d_1 \end{pmatrix} = 0, \tag{A 1}$$

together with $c_1 = e_1 = 0$. $\mathbf{L}_0$ is reduced to lower-triangular form after multiplication by a matrix whose first row is the vector

$$\mathbf{M}_0 = ((i\omega_0+1)(i\omega_0+\zeta),\ \sigma r^{(o)}(i\omega_0+\zeta),\ -\sigma\zeta q(i\omega_0+1));$$

multiplying (A 1) from the left by $\mathbf{M}_0$, we then recover the results (3.3) and (3.4). We are free to choose a_1 and normalize b_1 and d_1 to it:

$$a_1 = e^{i\omega\tau}, \quad b_1 = e^{i\omega\tau}/(i\omega_0+1), \quad d_1 = e^{i\omega\tau}/(i\omega_0+\zeta), \tag{A 2}$$

where only the real parts of the complex expressions have meaning. In second order in ϵ we then obtain

$$\mathbf{L}_0 \begin{pmatrix} a_2 \\ b_2 \\ d_2 \end{pmatrix} = \begin{pmatrix} -i\omega_1 a_1 + \sigma r_1^{(o)} b_1 \\ -i\omega_1 b_1 \\ -i\omega_1 d_1 \end{pmatrix} \tag{A 3}$$

and, multiplying by $\mathbf{M}_0$, we find that $r_1^{(o)} = \omega_1 = 0$. We may now set $a_2 = 0$, whence it follows that $b_2 = d_2 = 0$. In order to find c_2 and e_2 we must evaluate the nonlinear terms in (2.17*c*, *e*). It is convenient to retain the complex notation, which greatly

simplifies the algebra, without explicitly introducing sines and cosines. We therefore replace all products $z_1 z_2$ by $\frac{1}{2}z_1(z_2+z_2^*)$, where the star denotes a complex conjugate, and so obtain

$$c_2 = -\frac{1}{2(i\omega_0+1)}\left[1+\frac{\varpi e^{2i\omega\tau}}{2i\omega_0+\varpi}\right], \quad e_2 = \frac{\varpi}{2(i\omega_0+\zeta)}\left[\frac{1}{(4-\varpi)\zeta}+\frac{e^{2i\omega\tau}}{(4-\varpi)\zeta+2i\omega_0}\right]. \tag{A 4}$$

The quantities $r_2^{(o)}$ and ω_2 are now determined by the third-order solvability condition. We require that no secular terms be generated by the inhomogeneous terms proportional to $e^{i\omega\tau}$ in the equation

$$\mathbf{L}_0\begin{pmatrix}a_3\\b_3\\d_3\end{pmatrix} = \begin{pmatrix}-i\omega_2 a_1+\sigma r_2^{(o)}b_1+\sigma\zeta q(\varpi-3)d_1e_2\\-i\omega_2 b_1+a_1c_2\\-i\omega_2 d_1+a_1e_2\end{pmatrix}. \tag{A 5}$$

We apply the prescription for products, given above, to the right-hand side of (A 5), retaining only terms proportional to $\exp \pm i\omega\tau$, and, after multiplying the resulting vector by $\mathbf{M}_0$, we finally obtain a complex expression connecting ω_2 and $r_2^{(o)}$. This expression is conveniently simplified by using the identities

$$\sigma r^{(o)} = (\omega_0^2+1)\frac{\sigma+\zeta}{1-\zeta}, \quad \sigma\zeta q = (\omega_0^2+\zeta^2)\frac{\sigma+1}{1-\zeta} \tag{A 6}$$

to eliminate $r^{(o)}$ and q in favour of ω_0. We find that

$$\begin{aligned}2\omega_0\omega_2(1+\sigma+\zeta+i\omega_0)+\sigma r_2^{(o)}(i\omega_0+\zeta)&\\ = \frac{(\sigma+\zeta)(\zeta+i\omega_0)}{4(1-\zeta)}&\left[2+\frac{\varpi(1-i\omega_0)}{\varpi+2i\omega_0}\right]\\ -\frac{\varpi(\sigma+1)(1+i\omega_0)}{4(1-\zeta)}&\left[\frac{2(\varpi-2)}{4-\varpi}+\frac{(\varpi-2)\zeta-(4-\varpi)i\omega_0}{(4-\varpi)\zeta+2i\omega_0}\right].\end{aligned} \tag{A 7}$$

Expressions for ω_2 and $r_2^{(o)}$ can be obtained by forming real and imaginary parts of (A 7). We are particularly interested in the condition $r_2^{(o)} = 0$ which defines the transition between supercritical and subcritical bifurcation. This condition is given by a quadratic equation for ω_0^2, obtained by imposing the condition that ω_2 be real when $r_2^{(o)} = 0$:

$$\begin{aligned}&4\omega_0^4[2(1+\sigma)(\zeta+\sigma)(\varpi^3-11\varpi^2+16\varpi+16)-\varpi(4-\varpi)\{(\varpi+2)(\zeta+\sigma)\\&-(\varpi^2-6\varpi+12)\zeta(1+\sigma)\}]+\omega_0^2[\varpi(4-\varpi)\zeta\{(1+\sigma)(4\Delta+\varpi^2)(\varpi^2-6\varpi+12)\\&+(\zeta+\sigma)(6\varpi-\zeta(\varpi^3-6\varpi^2+4\varpi+28))\}+(1+\sigma)(\zeta+\sigma)\{2\varpi^2(\varpi^3-12\varpi^2+18\varpi+24)\\&+4\varpi(4-\varpi)(\varpi^2-7\varpi+13)\zeta-2(4-\varpi)^2(5\varpi^2-4\varpi-16)\zeta^2\}]\\&+\varpi(4-\varpi)\zeta[\Delta\{(1+\sigma)\varpi^2(\varpi^2-6\varpi+12)\\&-\zeta^2(\zeta+\sigma)(2+\varpi)(4-\varpi)^2\}-3\zeta(1+\sigma)(\zeta+\sigma)\varpi(4-\varpi)(\varpi^2-\varpi-4)]=0.\end{aligned} \tag{A 8}$$

If this equation has no real roots the Hopf bifurcation remains supercritical for all values of q. It is easy to confirm that $r_2^{(o)} > 0$ when $\varpi = 2$. For values of ϖ around 2 the bifurcation is always supercritical. However, for suitable choices of σ and ζ, subcritical oscillations can be found for both small enough and large enough values of ϖ $(0 < \varpi < 4)$.

REFERENCES

BUSSE, F. H. 1975 Nonlinear interaction of magnetic field and convection. *J. Fluid Mech.* **71**, 193–206.

CHANDRASEKHAR, S. 1961 *Hydrodynamic and Hydromagnetic Stability*. Oxford: Clarendon Press.

DA COSTA, L. N., KNOBLOCH, E. & WEISS, N. O. 1981 Oscillations in double-diffusive convection. *J. Fluid Mech.* **109**, 25–43.

DANIELSON, R. E. 1961 The structure of sunspot penumbras. II. Theoretical. *Astrophys. J.* **134**, 289–311.

FEIGENBAUM, M. J. 1978 Quantitative universality for a class of nonlinear transformations. *J. Stat. Phys.* **19**, 25–52.

FRANCESCHINI, V. 1980 A Feigenbaum sequence of bifurcations in the Lorenz Model. *J. Stat. Phys.* **22**, 397–407.

FRANCESCHINI, V. & TEBALDI, C. 1979 Sequences of infinite bifurcations and turbulence in a five-mode truncation of the Navier–Stokes equations. *J. Stat. Phys.* **21**, 707–726.

GALLOWAY, D. J. & MOORE, D. R. 1979 Axisymmetric convection in the presence of a magnetic field. *Geophys. Astrophys. Fluid Dyn.* **12**, 73–105.

HOPF, E. 1942 Abzweigung einer periodischen Lösung von einer stationären Lösung eines Differentialsystems. *Ber. Math. Phys. Sächs. Akad. Wiss.* **94**, 1–22 (trans. in Marsden & McCracken 1976, pp. 163–193).

HUPPERT, H. E. & MOORE, D. R. 1976 Nonlinear double-diffusive convection. *J. Fluid Mech.* **78**, 821–854.

JEANS, J. H. 1928 *Astronomy and Cosmogony*, pp. 179–186. Cambridge University Press.

KNOBLOCH, E. & PROCTOR, M. R. E. 1981 Nonlinear periodic convection in double-diffusive systems. *J. Fluid Mech.* **108**, 291–316.

LORENZ, E. N. 1963 Deterministic nonperiodic flow. *J. Atmos. Sci.* **20**, 130–141.

MARSDEN, J. E. & MCCRACKEN, M. 1976 *The Hopf Bifurcation and its Applications*. Springer-Verlag, New York.

POINCARÉ, H. 1885 Sur l'équilibre d'une masse fluide animee d'un mouvement de rotation. *Acta Math.* **7**, 259–380.

PROCTOR, M. R. E. & GALLOWAY, D. J. 1979 The dynamic effect of flux ropes on Rayleigh–Bénard convection. *J. Fluid Mech.* **90**, 273–287.

RUBENFELD, L. A. & SIEGMANN, W. L. 1977 Nonlinear dynamic theory for a double-diffusive convection model. *SIAM J. Appl. Math.* **32**, 871–894.

SATTINGER, D. H. 1973 *Topics in stability and bifurcation theory*. Lecture Notes in Mathematics, **309**. Springer-Verlag, Berlin.

SIEGMANN, W. L. & RUBENFELD, L. A. 1975 A nonlinear model for double-diffusive convection. *SIAM J. Appl. Math.* **29**, 540–557.

SPIEGEL, E. A. 1972 Convection in stars. II. Special effects. *Ann. Rev. Astron. Astrophys.* **10**, 261–304.

VERONIS, G. 1959 Cellular convection with finite amplitude in a rotating fluid. *J. Fluid Mech.* **5**, 401–435.

VERONIS, G. 1965 On finite amplitude instability in thermohaline convection. *J. Marine Res.* **23**, 1–17.

VERONIS, G. 1966 Motions at subcritical values of the Rayleigh number in a rotating fluid. *J. Fluid Mech.* **24**, 545–554.

WEISS, N. O. 1964 Convection in the presence of restraints. *Phil. Trans. Roy. Soc.* A **256**, 99–147.

WEISS, N. O. 1966 The expulsion of magnetic flux by eddies. *Proc. Roy. Soc.* A **293**, 310–328.

WEISS, N. O. 1977 Magnetic fields and convection. *Problems of Stellar Convection* (ed. E. A. Spiegel and J.-P. Zahn), pp. 176–187. Berlin: Springer-Verlag.

WEISS, N. O. 1981*a* Convection in an imposed magnetic field. Part 1. The development of nonlinear convection. *J. Fluid Mech.* **108**, 247–272.

WEISS, N. O. 1981*b* Convection in an imposed magnetic field. Part 2. The dynamical regime. *J. Fluid Mech.* **108**, 273–289.

WEISS, N. O. 1981*c* The interplay between magnetic fields and convection. *J. Geophys. Res.* (in press).